

# Zone Wise Local Characterization of Welds Using Digital Image Correlation: Uniform Stress and Virtual Fields Method

Saranath K.M.

A Thesis Submitted to  
Indian Institute of Technology Hyderabad  
In Partial Fulfillment of the Requirements for  
The Degree of Master of Technology



Department of Mechanical and Aerospace Engineering

June 2014

## Declaration

I declare that this written submission represents my ideas in my own words, and where ideas or words of others have been included, I have adequately cited and referenced the original sources. I also declare that I have adhered to all principles of academic honesty and integrity and have not misrepresented or fabricated or falsified any idea/data/fact/source in my submission. I understand that any violation of the above will be a cause for disciplinary action by the Institute and can also evoke penal action from the sources that have thus not been properly cited, or from whom proper permission has not been taken when needed.

Saranath

(Signature)

SARANATH.K.M

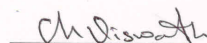
(Saranath K.M.)

ME12M1023


(Roll No.)

## Approval Sheet

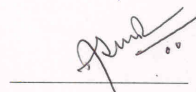
This Thesis entitled Zone Wise Local Characterization of Welds Using Digital Image Correlation: Uniform Stress and Virtual Fields Method by Saranath K.M. is approved for the degree of Master of Technology from IIT Hyderabad



(Dr. Viswanath Chinthapenta) Examiner  
Dept. of Mechanical and Aerospace Engg.  
IIT Hyderabad



(Dr. M. Ramji) Adviser  
Dept. of Mechanical and Aerospace Engg.  
IIT Hyderabad



(Dr. Abhay Sharma) Co-Adviser  
Dept. of Mechanical and Aerospace Engg.  
IIT Hyderabad



(Dr. S. Suriya Prakash) Chairman  
Dept. of Civil Engg.  
IIT Hyderabad

## Acknowledgements

I would like to extend my heartfelt appreciation and gratitude to a number of people, who helped in realizing this thesis work.

First and foremost, I would like to express deepest gratitude to my research advisor, Dr. M. Ramji, for his constant and continuous support throughout the period of my thesis work. He was very patient while going through my presentations and very supportive over the research ideas put forward by me. It has been my honour and privilege, working under him.

I would like to extend my heartfelt thanks to my co-advisor, Dr. Abhay Sharma, for those very creative advices and discussions, he had provided during my thesis work. He allowed me to use the facilities of Manufacturing lab under him, for carrying out various experimental analyses. Without him, it would have been impossible for me to complete this thesis.

I would like to thank Mr. Bongiri Rajkumar and Mr. Joshua Daniel for their help in the initial stage of my work. I am thankful to Mr. Moulali Syed and Mr. Dhananjay Sahoo of Manufacturing Lab for their support and suggestions on specimen preparation. Also I would like to acknowledge the support provided to me by Dr. Pinaki Prasad, Dr. Suhash Ranjan, Mr. Manish Meshram and Mr. Dan Sathiraj of Department of Material Science and Metallurgical Engineering for carrying out microhardness and micrographic examination.

I would like to thank Mr. Mohammad Kashfuddoja, Ms. R. Srilakshmi and Naresh Reddy Kolanu of Engineering Optics Lab for all the fruitful discussions, critical suggestions and the help extended in conducting tensile tests which intern helped me in the timely completion of this work. I am thankful to all my colleagues at Engineering Optics lab, Mr. Prataprao Patil, Mr. Jabir Ubaid, Mr. Vishwajeet Bhise, Mr. Lokeshwara Rao and Mr. Sourabh Khedkar for their valuable assistance in realizing this thesis. I would also thank all the staff of central workshop for helping me in specimen preparation and material management.

I would like to acknowledge Mr. Sreejith T V, Department of Electrical Engineering for the discussions on image correlation basics. His support was vital in the timely completion of this work. I would like to extend my heartfelt thanks to Ms. Karthika Vijayan, Department of Electrical Engineering for helping me with LaTeX document preparations and patiently correcting the manuscripts for publications.

Last but not the least I would like to thank my parents and sister for all those inspiring words upon my hard times during the period of my thesis work.

Saranath K.M.

# Dedication

*Dedicated to  
My Mother, Father and My Teachers*

## Abstract

The process of welding is associated with high and varying thermal gradients across the weld, resulting in inhomogeneous material properties surrounding the weldment. A proper understanding of the varying mechanical properties of the weld and surrounding materials is important in designing and modelling of components with weld. In the initial study the characterisation of different zones such as fusion zone, heat affected zones and unaffected base material of a deposited weld is carried out using uniform stress method (USM) involving digital image correlation (DIC) technique. A methodology using the micrographic observation and image processing is proposed for accurate identification of various weld zones. The response of welded samples in the elastic and plastic region is compared with the virgin sample. Full range stress-strain curves are obtained for each zone using the whole field strain measurement involving DIC. The parameters investigated are Young's modulus, Poisson's ratio, yield stress, strain hardening exponent and strength coefficient. A study regarding the variation of properties with respect to varying weld currents of 100 A, 130 A and 150 A is carried out. The Vickers micro hardness measurement is also conducted to obtain the variation in hardness across weldment. Fusion zone of all the welded samples have reported lower Young's modulus and higher yield strength compared to virgin samples. The Vicker's hardness values obtained for fusion and heat affected zones are in line with the yield stress variation obtained zone wise.

Further, local zone wise elastic and plastic characterization of electron beam welded Ti-6Al-4V titanium alloy is carried out using virtual fields method (VFM) and the results are compared with the results obtained using USM. The results obtained using USM and VFM are in good agreement. From the zone wise parameters it is observed that the fusion zone is having the least Young's modulus and exhibits higher Poisson's ratio, yield stress and strength coefficient. Base metal, where the specimens failed has reported the lowest yield stress value. Heat affected zones have recorded a higher strain hardening exponent in comparison with other zones. Vicker's microhardness examination across the weld also followed the same trend as that of zone wise parameters extracted, which reassured the accuracy of the implemented technique.

# Contents

Acknowledgements . . . . .	iv
Abstract . . . . .	vi
<b>1 Introduction and Literature Review</b>	<b>5</b>
1.1 Introduction . . . . .	5
1.1.1 Characterization of Welds . . . . .	7
1.1.2 Gas Metal Arc Welding (GMAW) . . . . .	8
1.1.3 Electron Beam Welding (EBW) . . . . .	9
1.1.4 Introduction to Digital Image Correlation . . . . .	10
1.2 Literature Review . . . . .	12
1.3 Scope and Motivation . . . . .	14
1.4 Thesis layout . . . . .	14
<b>2 Zone Wise Local Characterization of Welds Using Digital Image Correlation Technique</b>	<b>15</b>
2.1 Introduction . . . . .	15
2.2 Material and Welding Parameters . . . . .	16
2.3 Micrographic Examination . . . . .	17
2.4 Vickers Microhardness Testing . . . . .	18
2.5 Constitutive Parameter Estimation . . . . .	18
2.5.1 Specimen dimensions and Tensile Testing . . . . .	18
2.5.2 Zone Identification . . . . .	19
2.5.3 Constitutive Models and Parameter Estimation . . . . .	21
2.6 Results and Discussions . . . . .	23
2.6.1 Micrographic Examination . . . . .	24
2.6.2 Vicker's Microhardness Measurement . . . . .	25
2.6.3 Constitutive Parameters . . . . .	26
2.7 Closure . . . . .	31
<b>3 Investigation of local zone wise elastic and plastic properties of electron beam welded Ti-6Al-4V alloy using DIC</b>	<b>35</b>
3.1 Introduction . . . . .	35

3.2	Experimental Procedure . . . . .	36
3.2.1	Welding and Specimen Preparation . . . . .	36
3.2.2	Micrographic Examination . . . . .	37
3.2.3	Vicker's Microhardness Measurement . . . . .	38
3.2.4	Tensile Testing and Digital Image Correlation . . . . .	38
3.3	Parameter Extraction and Material Model . . . . .	40
3.3.1	Zone Identification . . . . .	40
3.3.2	Material Model . . . . .	41
3.4	Solution Methodology . . . . .	42
3.5	Results and Discussion . . . . .	42
3.5.1	Vicker's Microhardness . . . . .	43
3.5.2	Tensile Test Results and Constitutive Parameters . . . . .	43
3.6	Closure . . . . .	48
<b>4</b>	<b>Local characterization of welds using virtual fields method involving DIC</b>	<b>50</b>
4.1	Introduction . . . . .	50
4.2	Material Model . . . . .	51
4.3	Weld Zone Identification . . . . .	51
4.4	Virtual Fields Formulation . . . . .	53
4.4.1	Elastic Parameter Identification . . . . .	54
4.4.2	Plastic Parameter Identification . . . . .	57
4.5	Results and Discussions . . . . .	58
4.5.1	Observations From Tensile Test . . . . .	58
4.5.2	Local parameters using USM and VFM . . . . .	59
4.6	Closure . . . . .	63
<b>5</b>	<b>Conclusions and Future Recommendations</b>	<b>64</b>
5.1	Conclusions . . . . .	64
5.2	Future Recommendations . . . . .	65
	<b>Appendices</b>	<b>66</b>
<b>A</b>	<b>Zone Wise Parameters Obtained for Ti-6Al-4V EBW Sample Using USM</b>	<b>67</b>
<b>B</b>	<b>Zone Wise Parameters Obtained for Ti-6Al-4V EBW Sample Using VFM</b>	<b>68</b>
	<b>References</b>	<b>69</b>



# List of Figures

1.1	Schematic diagram showing various zones in the cross-section of a weld deposition . . . . .	5
1.2	KUKA <sup>®</sup> twin wire robotic welding station used in this study for making GMAW welds. . . . .	9
1.3	Schematic of electron beam welding. (a) Process (b) Keyhole. <i>Image courtesy:</i> Sindo K., Welding Metallurgy, Wiley Interscience, 2003 . . . . .	10
1.4	Schematic of subset matching DIC: (a) undeformed and (b) deformed. . . . .	11
2.1	Top view of weld deposition made with different current ratings. (a) with 100 A (b) with 130 A and (c) with 150 A. . . . .	17
2.2	Optical microscopic image of an etched sample of 150 A weld at 5x magnification. . . . .	18
2.3	Optical microscope images of etched samples at various magnifications. (a) fusion zone at 5x zoom. dendrite structure can be identified. (b),(c) fusion zone at 10x zoom. (d),(e) fusion zone with dendrite structures at 50x zoom. (f) Heat affected zone at 50x zoom. All these images belong to weld zone of 150 A specimen. . . . .	19
2.4	Figure showing measurement locations. (a) Coordinates of the points marked 'X' are measured using Optical microscope. (b) Vickers micro hardness testing carried out in the thickness (line AB) and length direction (line CD), where C is the center of fusion zone. . . . .	20
2.5	Specimen geometries used for characterisation (a) orientation of the specimen with respect to the weld (b) dimension of the tensile specimen. . . . .	20
2.6	Weld specimens used for testing (a) specimens without speckle pattern (b) specimens with speckle pattern. . . . .	21
2.7	Experimental set up involving DIC (a) overall set up (b) zoomed view of the gripped specimen with extensometer attached. . . . .	22
2.8	Longitudinal strain ( $\epsilon_{yy}$ ) obtained using DIC at different load levels over the weld zone for the 130 A specimen. . . . .	23

2.9	Zone identification using strain distribution. (a) longitudinal strain ( $\epsilon_{yy}$ ) contours during the plastic deformation of a 130 A specimen estimated at a load of 11.5 kN (b) ( $\epsilon_{yy}$ ) distribution along the line shown in Fig. 2.9(a), divided into various zones. . . . .	24
2.10	Images with pixels highlighted for various weld zones in 150 A specimen (a) fusion zone (b) coarse grain HAZ (c) fine grain HAZ 1 (d) fine grain HAZ 2. Pixels apart from these zones are considered as base metal. . . . .	25
2.11	Processes involved in parameter extraction for local weld zones involving DIC	26
2.12	Depth of weld penetration for different current ratings. . . . .	27
2.13	Vickers micro hardness measurement across weld zone. (a) Variation of $HV_{0.3}$ in thickness direction. (b) Variation of $HV_{0.3}$ along longitudinal direction. . . . .	27
2.14	Fractured specimens after tensile testing. Current rating used for welding is mentioned on the samples. . . . .	28
2.15	Stress - strain curves obtained from the extensometer reading. . . . .	29
2.16	Stress-strain curve obtained using data from DIC technique (a) virgin sample (b) 100 A (c) 130 A (d) 150 A. . . . .	30
2.17	Comparison of yield stress estimated using extensometer (EM) readings and DIC. . . . .	31
2.18	Yield stress and maximum strain variation across the weld zone (a) yield stress (b) maximum strain. . . . .	31
2.19	Linear and non linear curves fitted on experimental data for parameter extraction corresponding to the fusion zone of 130 A specimen. . . . .	32
2.20	Comparison of Young's modulus estimated using extensometer (EM) readings and DIC . . . . .	32
2.21	Variation of Young's modulus across weld zones for specimens with different current ratings. . . . .	33
2.22	Variation of strain hardening exponent and strength coefficient across weld zones for specimens with different current ratings (a) strain hardening exponent (b) strength coefficient. . . . .	33
2.23	Variation of Poisson's ratio across weld zone for specimens with different current ratings. . . . .	33
3.1	Welded sheet with tensile specimen orientation. . . . .	37
3.2	Tensile specimens with weld. (a) tensile specimens showing the AOI and weld (b) specimen dimensions. . . . .	37
3.3	Microstructure of EBW at 5x magnification. Various weld zones are tagged in the figure. . . . .	38
3.4	Zoomed view of the microstructure of different weld zones. (a) base metal at 20x magnification (b) FZ, HAZ and base metal at 5x magnification (c) FZ at 20x magnification. . . . .	39

3.5	Schematic showing the hardness measurement location. Microhardness values are measured along line AB of length 8 mm. . . . .	40
3.6	Experimental set up involving DIC (a) overall set up (b) specimen with speckle pattern. . . . .	40
3.7	Strain evolution and divided AOI (a)Longitudinal strain distribution at various load levels (b) AOI divided into various zones . . . . .	41
3.8	Vicker’s microhardness variation across weld zones. . . . .	43
3.9	Fractured specimens after tensile testing. . . . .	44
3.10	Global stress-strain curves obtained using extensometry and DIC technique. . . . .	44
3.11	Variation of $\varepsilon_{yy}$ across the weld (a) figure showing line AB along which strain values are collected (b) $\varepsilon_{yy}$ variation along line AB. . . . .	45
3.12	Zone wise full range stress-strain curves obtained using DIC technique. . . . .	45
3.13	Linear and non linear curves fitted on experimental data for parameter extraction corresponding to zone 6. . . . .	46
3.14	Zone wise variation in Young’s modulus. . . . .	47
3.15	Zone wise variation in Poisson’s ratio. . . . .	47
3.16	Zone wise variation in yield stress. . . . .	48
3.17	Zone wise variation in strength coefficient. . . . .	48
3.18	Zone wise variation in strain hardening exponent. . . . .	49
4.1	Strain evolution and divided AOI (a)Longitudinal strain distribution at various load levels (b) AOI divided into various zones . . . . .	52
4.2	Diagram showing the loading and boundary conditions of the tensile testing. ‘AOI’ is the section of specimen where the strains are measured. . . . .	53
4.3	Fractured specimens after tensile testing. . . . .	58
4.4	Comparison of zone wise variation in Young’s modulus obtained using USM and VFM. . . . .	59
4.5	Comparison of zone wise variation in Poisson’s ratio obtained using USM and VFM. . . . .	60
4.6	Comparison of zone wise variation in strength coefficient obtained using USM and VFM. . . . .	61
4.7	Comparison of zone wise variation in strain hardening exponent obtained using USM and VFM. . . . .	62
4.8	Comparison of zone wise variation in yield stress obtained using USM and VFM. . . . .	62

# List of Tables

2.1	Chemical composition of mild steel sheet . . . . .	16
2.2	Details of welding methodology and parameters . . . . .	16
2.3	Percentage variation between maximum and base material hardness for specimens with different current ratings. . . . .	28
2.4	Obtained values of elongation and ultimate tensile strength for different weld specimens. . . . .	29
2.5	Percentage increase of yield stress in comparison with virgin sample. . . . .	31
2.6	Percentage variation of Young’s modulus in comparison with virgin sample. . . . .	32
3.1	Details of welding methodology and parameters . . . . .	37
3.2	Length of various zones which are identified in Fig. 3.7(b) . . . . .	41
3.3	Global properties of the weld using Extensometry and DIC technique . . . . .	44
4.1	Length of various zones which are identified in Fig. 4.1(b) . . . . .	52
4.2	Percentage deviation of zone wise Young’s modulus extracted using VFM from that of extracted using USM . . . . .	60
4.3	Percentage deviation of zone wise Poisson’s ratio extracted using VFM from that of extracted using USM . . . . .	60
4.4	Percentage deviation of zone wise strength coefficient extracted using VFM from that of extracted using USM . . . . .	61
4.5	Percentage deviation of zone wise strain hardening exponent extracted using VFM from that of extracted using USM . . . . .	61
4.6	Percentage deviation of zone wise yield stress extracted using VFM from that of extracted using USM . . . . .	63
A.1	Zone wise parameters extracted for Ti-6Al-4V EBW Sample Using USM . . . . .	67
B.1	Zone wise parameters extracted for Ti-6Al-4V EBW Sample Using VFM . . . . .	68

# Chapter 1

## Introduction and Literature Review

### 1.1 Introduction

Welding is an inevitable material joining technique in most of the engineering and fabrication process. In a welding operation, energy required for creating chemical bonds between the materials to be joined is obtained either from heat, pressure or from the combined action of heat and pressure [1]. The heat source interaction time and thermal gradient developed across the weld will give rise to material zones with different micro-structure compared to parent material [2]. Because of this micro-structural change the behaviour of various zones like fusion zone (FZ), heat affected zones (HAZs) and base material (BM) will be different from one another. Refer Fig. 1.1 for a schematic view of the cross-section of a weld deposition. The formation of these zones make a welded specimen heterogeneous in microstructure and hence complex in mechanical response upon loading. Global response of a welded component against loading is a function of local property distribution associated with this heterogeneous structure. In a perfect weld the variation of mechanical properties of FZ and HAZs will be close to that of the base metal. Process of welding is associated

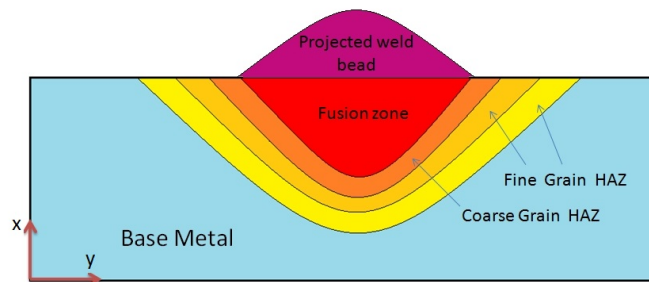


Figure 1.1: Schematic diagram showing various zones in the cross-section of a weld deposition

with many parameters such as welding methodology, heat source interaction time, distance between the electrode and work piece, power density, feed rate, shielding techniques, environmental factors etc. Any changes made to the above parameters will result in a unique weld zone microstructure and hence distinct property variations. A proper understanding of these varying constitutive parameters is important in following aspects:

- Identification of the weak zone and validation of the design requirements of the components comprises of welds.
- Modelling of complicated welded components where component level experimental stress analysis is difficult.
- Optimizing welding parameters and selecting proper welding technique to produce components with required design characteristics.
- Design manufacturing operations such as forming of a welded sheet metal to minimize the defects in the final product.

In this study, zone wise local extraction of elastic and plastic properties of welds are attempted. Two different methodologies involving Digital image correlation (DIC) is utilized for parameter extraction. One is uniform stress method (USM) through which zone wise full range stress-strain curves are extracted and from those curves elastic and plastic parameters are identified. Second one is by using virtual fields method (VFM) and here a more computationally fast and accurate zone wise parameter extraction is materialized using the weak form of equilibrium equations generated using principle of virtual work. Chapter wise description on the implementation of above methodologies are as follows.

The objective of the study described in chapter 2 is accurate identification and characterization of various thermally affected zones and obtain the full range stress-strain curves corresponding to each identified zones of a gas metal arc weld (GMAW) on mild steel sheet . Characterization includes identification of different zones, finding out the constitutive parameters of each zone within the elastic region, estimation of yield stress in various zones and further strain hardening exponent and strength coefficient as specified by Hollomon's power law. DIC is employed for obtaining whole field strain distribution in various zones across the weldment. Vickers microhardness measurement is also carried out on various zones in order to capture the variation of surface hardness across the weldment. The main difficulty in incorporating DIC is on the method of discretizing the weld area into different zones. A strain based method coupled with the microstructure examination is proposed and used in this study for identification of various zones. In order to study the effect of variation of welding parameters on the local properties, specimens are fabricated using three different current ratings such as 100 A, 130 A and 150 A by keeping other welding parameters constant.

Chapter 3 elaborates on the zone wise extraction of elastic and plastic parameters of electron beam welded (EBW) Ti-6Al-4V titanium alloy sheets using DIC technique. Various zones such as FZ, HAZs and BM are identified from the micrographic examination of the weld. Transverse weld tensile samples are tested and by using DIC the surface strain distribution across the weld is measured. The surface strain distribution is divided in to various zones based on the informations from the micrographic study and then zone wise full range stress-strain curves are extracted. Required material parameters are extracted from these zone wise stress-strain curves. Young's modulus and Poisson's ratio are the elastic parameters which are extracted. Hollomon's power law is used here as the material model for the plastic parameter extraction and the sought parameters are strength coefficient and strain hardening exponent. Another important parameter extracted is the zone wise yield stress from that information the weakest zone is identified. Extensometry technique is also employed to get an average response of the weld. Vicker's microhardness values are measure across the weldment to get the variation in microhardness from zone to zone and to compare the trend in hardness variation with extracted parameters.

Chapter 4 is on the implementation of VFM towards zone wise local characterization of EBW on Ti-6Al-4V titanium alloy. Input data for the analysis is derived from the same test data used for the analysis in chapter 3. For the first time both elastic and plastic parameters are extracted using VFM for each weld zone. In this study, the results obtained in chapter 3 is recalculated using VFM for comparing it with USM methodology.

Since this study is dealing with characterization of welds (GMAW and EBW) and DIC technique is used for measuring the surface strain distribution, following subsections are included as a brief introduction into weld zone characterization, GMAW, BEW and DIC.

### **1.1.1 Characterization of Welds**

There are many methods available for characterizing a weld depending on the application, function and required properties of the weld. Characterization can be done at three different levels. First level is based on the informations gathered using non destructive type examinations. Visual inspections, radiography, ultrasonic testing, and liquid penetrant inspection are utilized here to quantify the surface and internal defects. Based on the severity of the defects the welds are characterized. But this type of inspection is not capable of providing any information about the micro structure and zone wise mechanical properties of a weld. Second level of weld characterization is a destructive method by which the micro structural changes across the weld is visualized. In this, a small section of weld is taken from the weld and based on the requirement various analysis are performed such as examination of weld bead size, bead shape, weld homogeneity, orientation of beads in a multipass weld, micro-segregation, grain structure and its size measurement and compositional analysis for finding the chemical composition and corrosion behaviour of the weld. In design stand point the above analysis are not sufficient to satisfy the requirements of a designer. In order to

validate a design which composed of weld, one require the mechanical properties associated with the welded component. So the third and important level of weld characterization is extraction of mechanical properties of a weldment. This level of characterization is the main aim of this thesis. Yield strength, tensile strength, ductility, hardness, and impact or fracture toughness are the typical mechanical properties which are extracted for characterizing a weld. Since a weld is composed of zones having varying microstructure these properties can differ from zone to zone. If the mechanical properties are extracted by considering all the zone combined together as a single zone, then the extracted property is known as global property of the weld. The properties associated with each weld zone are known as local properties. A main concern regarding the local properties of welds is the direct comparison of the same with base material properties. The aim is to ensure that the weld is not the weakest component of a structure and if it is the case then to compensate for this in the design. There are various methods available for extracting both global and local properties of a weld and they are summarized in section 1.2.

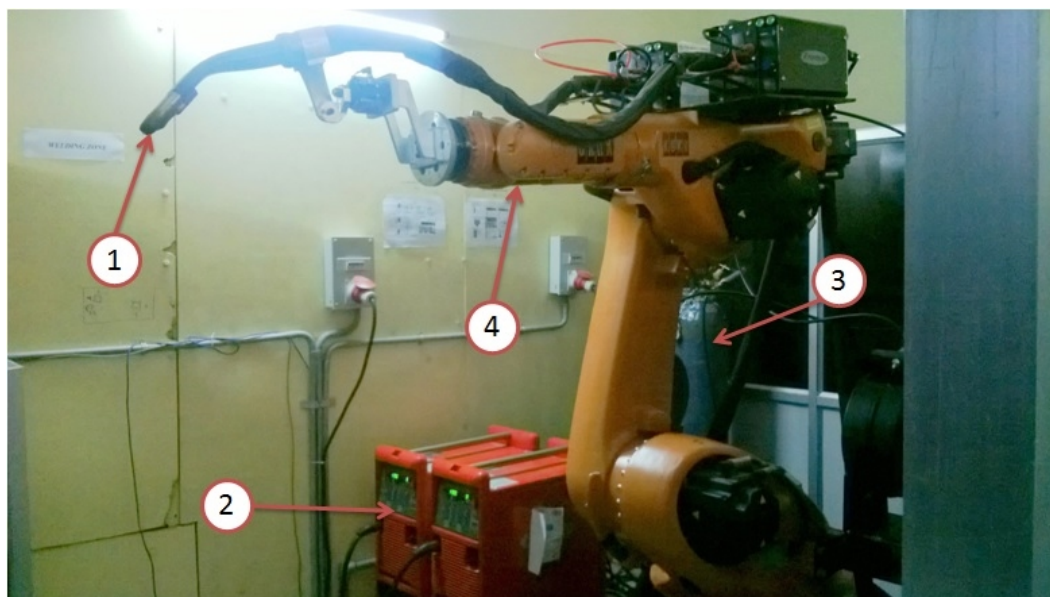
### **1.1.2 Gas Metal Arc Welding (GMAW)**

The concept of GMAW was introduced in 1920s and came to commercial usage from 1940s [2]. In this technique a continuously fed electrode of filler material is used to establish an arc between electrode and work piece. An externally supplied inert gas or a gas mixture is used for shielding the arc and fused metal. The primary objective of the shielding gas is to prevent the weld pool from reacting with atmospheric nitrogen and oxygen. The ionization potential of the gas also have an impact on the arc stability and gases with low ionization potential like argon can offer good arc stability and a chemically inert atmosphere. Carbon dioxide mixed with argon is a widely used shielding gas combination where the function of CO<sub>2</sub> is to provide more thermal conductivity to the shielding gas so that a more even distribution of heat to the work piece takes place. Higher speed, better deposition rate, more depth of penetration and ability to weld long welds and minimal postweld cleaning requirement because of the absence of a heavy slag are the major attractions of this welding technique.

For the study described in chapter 2 twin wire gas metal arc welding process is used for making heavy weld deposit and Fig. 1.2 shows the twin wire welding station. This welding technique uses two consumable wires simultaneously for arc production and filler metal deposition. Because of the advancements in the control technology for welding power controlling, the twin wire arc welding has become more flexible. This flexibility allows the user to independently select and control the electric potentials of each wire so that more stable weld conditions are achieved. When the independent power control is also incorporated into a twin wire arc welding system, then the process is known as tandem welding [3]. This technique has got several advantages over the single wire GMAW and conventional arc welding. It is successfully employed in welding cladding, and in special



applications such as brazing or combined brazing and welding [4]. It has got high production rates compared to conventional single wire welding [5, 6] and shows stable metal transfer with low welding current and lesser heat transfer to the base metal [7].



- |                           |                                 |
|---------------------------|---------------------------------|
| 1. Welding torch          | 2. Power source and controllers |
| 3. Shielding gas cylinder | 4. Robotic arm                  |

Figure 1.2: KUKA<sup>®</sup> twin wire robotic welding station used in this study for making GMAW welds.

### 1.1.3 Electron Beam Welding (EBW)

EBW is a high energy density fusion process which utilizes focused beam of electrons having very high velocities (0.3 to 0.7 times the speed of light). The kinetic energy of the electrons bombarding the work piece is instantaneously converted in to thermal energy which melts the surface layers and create path for the electron beam to further penetrate into the work piece. This will create a molten weld pool in the thickness direction and produces desired weld joint coalescence. Fig. 3.1 shows the schematic diagram of an EBW process. The working principle of EBW is: When the negatively charged electron gun (cathode) is heated above its thermionic emission temperature it emits electrons. Negatively charged bias electrode and anode helps to accelerate the electrons. When this electrons pass through the hole in the anode they are focused by an electromagnetic coil to the desired point of the specimen surface. This beam of high density electrons melts and vaporizes the specimen material to produce a key hole (ref Fig. 3.1) along the thickness. When the beam moves forward the surrounding specimen material melts and create a welded joint.

There are several advantages for EBW over conventional arc welding. They are, the ability to achieve higher depth of penetration which avoid the requirement of multiple

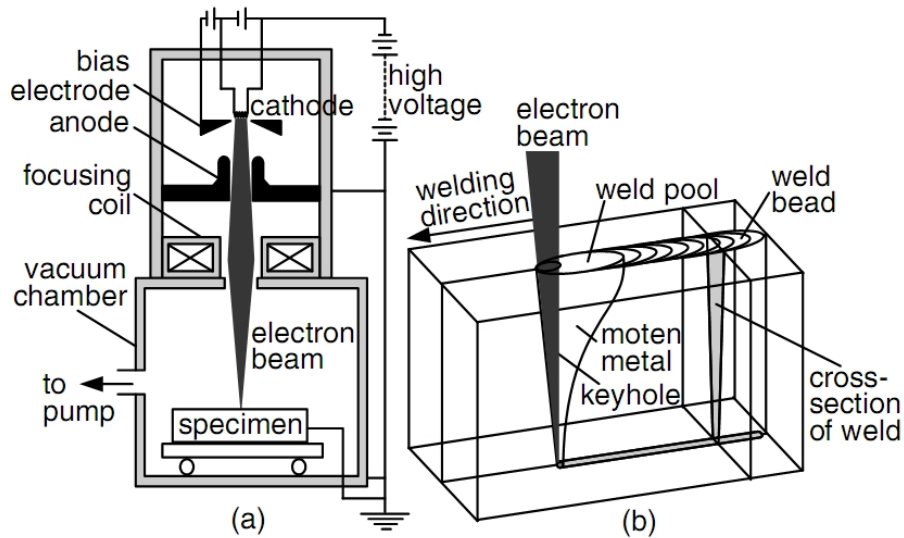


Figure 1.3: Schematic of electron beam welding. (a) Process (b) Keyhole. *Image courtesy: Sindo K., Welding Metallurgy, Wiley Interscience, 2003*

passes as in case of arc welding, narrow HAZ because of the lesser heat input during weld, the requirement of vacuum helps to use this technique for joining reactive metals. Welds produced using EBW have lesser distortion and shrinkage. The disadvantages are the cost of EBW setup which is in a higher side compared to the conventional arc welding, the high cost and time consumption for the tooling because the welding is materialized using a narrow electron beam which necessitate precise joint gap and positioning of the specimen. The requirement of vacuum chamber also creates limitations on the size of work piece can be welded using this technique.

#### 1.1.4 Introduction to Digital Image Correlation

DIC is a reliable non contact optical technique used in experimental mechanics for getting whole field displacement and strain fields. This technique came into existence from 1980's pioneered by Sutton's group [8, 9]. Its working principle is based on image comparison of the specimens coated with a random speckle pattern. Speckle patterns are nothing but random black dots sprayed over the specimen painted with white paint. Displacement fields are obtained by comparing the gray scale values of pixels subsets of the deformed specimen with the reference (undeformed) image of the specimen using a pattern matching algorithm. The pattern matching is based on obtaining maximum correlation between subsets of the image in the undeformed and deformed states (see Figure 1.4). A correlation function used for matching purpose is shown in Equation 1.1. The displacement of the centre of pixel subset is returned when a best match is identified. The strain fields are obtained by numerically differentiating the smoothed displacement fields.

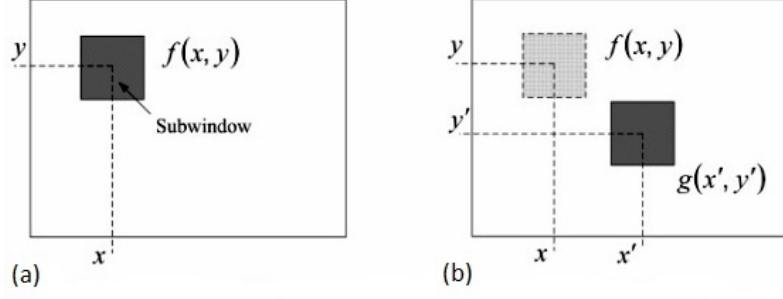


Figure 1.4: Schematic of subset matching DIC: (a) undeformed and (b) deformed.

$$C(u, v) = \frac{\sum_{i=1}^m \sum_{j=1}^m [f(x_i, y_i) - \bar{f}][g(x'_i, y'_i) - \bar{g}]}{\sqrt{\sum_{i=1}^m \sum_{j=1}^m [f(x_i, y_i) - \bar{f}]^2} \sqrt{\sum_{i=1}^m \sum_{j=1}^m [g(x'_i, y'_i) - \bar{g}]^2}} \quad (1.1)$$

where

$$x' = x + u_0 + \frac{\partial u}{\partial x} dx + \frac{\partial u}{\partial y} dy \quad (1.2)$$

$$y' = y + v_0 + \frac{\partial v}{\partial x} dx + \frac{\partial v}{\partial y} dy \quad (1.3)$$

$\bar{f}$  = Mean intensity value of reference subset

$\bar{g}$  = Mean intensity value of deformed subset

$m$  is the width of subset in pixels and  $u_0, v_0$  are translations of the centre of the subset in the  $x$  and  $y$  directions.

A single camera can be used for grabbing images towards measuring in-plane surface displacements and strain and this configuration is known as 2D DIC. For getting out-of-plane displacement, one can use two cameras for simultaneously grabbing images and this system configuration is known as 3D DIC. In case of 3D DIC, a detailed calibration procedure needs to be done to synchronise the cameras and three dimensional location of the object for estimating displacement components [10]. For a detailed understanding on the development, theory and capabilities of DIC, readers are advised to refer the following literatures [8–15]. In this study, a 2D-DIC system is used for measuring the surface strain fields of the weld samples. Post processing of the images is carried out using the commercially available image correlation software, Vic-2D [16]. A subset size of 29 pixels and a step size of 5 pixels are used for post processing.

There are many factors which can affect the displacement and strain estimate by a 2D DIC system. The main sources of the error in the estimate are intensity interpolation, image noise, lens distortion and out-of-plane displacements. Schreier *et al.* [17] have concluded that the intensity interpolation which is required for increasing the measurement resolution

can introduce errors of the order  $10^{-4}$  in the strain estimates. Pan [18] have suggested pre-smoothing the images using a Gaussian low-pass filter to reduce image noise based errors on the calculated strain field. In order to minimize the effect of out-of-plane displacements, Sutton *et al.* [19] have recommended to keep an approximate distance of 1.5 meters between the camera and the specimen while maintaining the perpendicularity between the line of sight and specimen surface. Choice of subset size also plays an important role in minimizing the error. The size of the subset is related to the average size of the speckles because for a better correlation each subset must contain adequate speckles to give distinct patterns [16].

## 1.2 Literature Review

The traditional method for estimating the property variation across the weld is hardness measurement. Instrumented ball indentation techniques and Vickers microhardness measurements are widely used to get the variation in hardness of various zones of weld [20–22]. But hardness measurement is confined to the response of the surface layer of the specimen material and there are no precise relationships available relating the constitutive parameters and hardness values. Another method is testing of micro-tensile samples made from different zones of a weld [23]. In practice the preparation of micro-tensile specimen is time consuming and the spatial resolution and accuracy achievable is also limited. Zuniga *et al.* [24] have proposed testing of bulk material produced by weld thermal simulation. However, it is difficult to model accurately the highly transient thermal gradients experienced by the weld zones.

Digital image correlation (DIC) technique is successfully used by many researchers to characterise the heterogeneous weld zones. DIC is an innovative whole field non-contact optical technique used for measuring strain and displacement in components over a wide range of length scales. This technique is easy to use since it involves simpler surface preparation of specimens and it can be applied to all kind of materials [25]. Lockwood *et al.* [26] and Leitão *et al.* [27] have simulated the global response of a friction stir weld using local constitutive behaviour obtained with DIC. Duvall and Reynolds [28, 29] have used DIC for the determination of weld and base metal constitutive behaviour with isostress assumption, but a clear strategy to get the size and shape of weld zones from speckled image has not been discussed. Sutton *et al.* [19] have compared both uniform stress and virtual fields methods for parameter identification of welded specimen and concluded that the uniform stress assumption is giving results with reasonable accuracy. Acar *et al.* [30] have studied the variation in mechanical properties of a multi-pass weld using DIC. Longitudinal strain and 0.2% proof stress are evaluated along a line passing through the weldment. Plastic zone behaviour and strain hardening effects have not been considered as part of their study. Strycker *et al.* [31] have attempted measuring of welding deformations by using DIC but constitutive parameter extraction has not been attempted. Yan *et al.* [32] have successfully

implemented DIC for studying the variation of strain across a pipeline weld. The distribution of stress at 0.2% strain in the vicinity of the weld is studied and has concluded that the weld nugget is experiencing higher levels of stress at 0.2% strain.

Song *et al.* [33] have reported the variation of Young's modulus and Poisson's ratio across the weld of electron beam welded TA15 Titanium alloy using ultrasonic method, where the Young's modulus value is found to be decreased from base metal towards weld nugget where as Poisson's ratio value is increasing. A similar observation is reported by Ambriz *et al.* [22], where an instrumented indentation test on the weld zone of a 6061-T6 aluminium alloy subjected to the modified indirect electric arc welding technique showed a lower Young's modulus value for the fusion zone of the weld compared to the base metal.

The advancements in non contact type whole field strain measurement systems such as DIC and the development of virtual fields method (VFM) have paved way for a more advanced method for identifying constitutive parameters. VFM, is a technique based on principle of virtual work (PVW) where the actual whole field strains and kinematically admissible virtual displacement fields are employed for identification of unknown parameters. This method utilizes PVW to write the weak form of local equilibrium equations which is nothing but those equations along with force boundary conditions [34], which form the basis of VFM. In elasticity problems, the unknown constitutive parameters are extracted by solving a linear system of equations which is formulated by selecting number of independent and kinematically admissible virtual displacement fields equal to the number of unknown parameters. Over the years since it's development, there are many fields in which VFM has been successfully implemented. A general review on the history, development and basic principles of VFM can be found in Ref. [35]. Avril *et al.* have recently published a review paper summarising various numerical / analytical technique which are coupled with full field strain measurements [36]. Pierron *et al.* [37], have used VFM and surface strain measurements of a thick composite coupon subjected to a shear-bending load and estimated the four through-thickness moduli. The stability of the method has also been checked in their study by adding simulated experimental noise and it is found to be stable except for Poisson's ratio measurement. Grédiac *et al.* [38], have proposed special virtual fields for the direct determination of material parameters using VFM.

Toussaint *et al.* [39] have introduced VFM with piecewise virtual fields for estimating the properties of a heterogeneous material. Further Grédiac *et al.*[40] have proposed VFM for identification of elasto-plastic constitutive parameters using whole field in-plane strain data. Sutton *et al.* [19] have applied VFM for identification of heterogeneous property variation across various weld zones of a pipe line girth weld and compared the results with uniform stress method (USM). They have concluded that the results obtained from USM is comparable to that of VFM and also the results indicate that the weld nugget possesses higher yield stress compared to other weld zones. In that study the yield stress estimated by VFM is on a lower side as compared to USM. Louédec *et al.* [41] have studied the local

elasto-plastic behaviour of friction stir welds (FSW) at different strain rates using VFM. They have indicated that there is a significant reduction in yield stress and hardening modulus in the nugget region which is as expected for a FSW weld.

### 1.3 Scope and Motivation

There exist many potential applications for the local characterization weld like identification of the mechanical properties of the weakest zone for design calculations, modelling of welds on complicated geometries by using the zone wise material properties, Optimization studies for selecting suitable welding parameters to obtain desired properties for the weld etc. There are lot of literatures available on characterisation of welds for its mechanical properties. But the established methods are time consuming and accurate zone wise extraction of varying elastic and plastic parameters of a weld is still an area where lot of improvements are required. Existing methods for zone wise characterization like micro hardness and miniature specimen testing have drawbacks like fewer informations from a single test, time consuming specimen preparations, lesser spatial resolution etc. Recently, DIC technique is used for characterization of the weld by few researchers and the area still hold lot of space for new research. The identification of various zones from the speckled images used for DIC is a challenge. So the identification of zones and extracting the zone wise constitutive parameters are attempted in chapter 2. Third chapter adopts the methodology used in chapter 2 for solving zone wise mechanical properties of an electron beam welded Ti-6Al-4V titanium alloy. The motivation for chapter 4 is the implementation of virtual fields method towards faster and accurate identification of zone wise elastic and plastic properties of a weld.

### 1.4 Thesis layout

Chapter 1 gives idea on the local zone wise characterisation of welds, Literature review on weld zone characterization, Various welding techniques used in this study, basics of DIC and Scope and motivation for this thesis.

Chapter 2 describes the implementation of DIC for local elastic and plastic parameter extraction of weld using USM. Methodology, zone identification using DIC and micrograph, Tensile testing and the results from testing of a GMAW weld on mild steel are discussed in detail.

Chapter 3 implements the method utilized in chapter 2 for characterizing the weld zones of a Ti-6Al-4V titanium alloy welded using EBW.

Chapter 4 deals with virtual field method for local characterization of welds. The results obtained in chapter 3 is compared with that of extracted using VFM.

Chapter 5 Summarizes and concludes the contributions of this work and future recommendations are discussed.

## Chapter 2

# Zone Wise Local Characterization of Welds Using Digital Image Correlation Technique

### 2.1 Introduction

Process of welding is associated with high and varying thermal gradients across the weld. These thermal gradients will result in microstructural changes and inhomogeneous material properties surrounding the weldment. The response of the welded structure against loading will be a function of these local properties. A proper understanding of the varying mechanical properties of the weld and surrounding materials is important in designing and modelling of components with weld. Also identification of failure zone yield stress is very important in structural design standpoint. In the present study the characterisation of different zones such as fusion zone, heat affected zones and unaffected base material of a deposited weld is carried out using digital image correlation (DIC) technique. Twin wire gas metal arc welding is used for weld deposition. The main difficulty in incorporating DIC is on the method of discretizing the weld area into different zones. A strain based method coupled with the microstructure examination is proposed and used in this study for identification of various zones. The response of the welded samples in the elastic and plastic region is compared with the virgin sample. Full range stress-strain curves are obtained for each zone using the whole field strain measurement involving DIC. Hollomon's power law is used for characterizing the plastic response. The parameters investigated are Young's modulus, Poisson's ratio, yield stress, strain hardening exponent and strength coefficient. A study regarding the variation of properties with respect to varying weld current of 100 A, 130 A and 150 A is also carried out. The Vickers micro hardness measurement is also conducted to obtain the variation in hardness across the weldment.

The rest of this chapter is organized as follows: Section (2.2) explains about the material

and welding technique used in this study. Section (2.3) describes about the micrographic examination of weldments to identify various thermally affected regions. Section (2.4) elaborates on the procedure adopted for finding the Vicker’s micro hardness across the weld. Section (2.5) discusses in detail on the methodology adopted in this study for extracting constitutive parameters using DIC. Results and other observations are discussed in section (2.6) and section (2.7) is closure.

## 2.2 Material and Welding Parameters

Mild steel sheets of 300 x 300 x 5 mm<sup>3</sup> are used as the base material from which specimens are manufactured. Bead-on-plate technique is used for producing weldments. The composition of the mild steel sheet examined using X-ray fluorescence technique is given in Table 2.1. The weld depositions are supposed to mimic the characteristics of a butt welded joint. Details of the welding technique and weld parameters are given in Table 2.2. KUKA twin

Table 2.1: Chemical composition of mild steel sheet

Element	Quantity in %	Element	Quantity in %
Na	0.326	V	0
Mg	0.035	Cr	0.041
Al	0.076	Mn	0.753
Si	0.371	Fe	97.738
P	0.003	Co	0.310
S	0.022	Ni	0.044
Cl	0.064	Cu	0.036
K	0.015	Zn	0.013
Ca	0.011	Eu	0.094
Sc	0	Yb	0.018
Ti	0.014	Re	0

wire robot welding station is used for producing the weld depositions on three different sheets with 100 A, 130 A and 150 A current ratings. During welding, all other parameters apart from the current are kept constant. No pre and post weld heat treatment are done. Weld beads produced are shown in Fig. 2.1.

Table 2.2: Details of welding methodology and parameters

Parameters	Values
Method	Twin wire gas metal arc welding
Gas	Argon+CO <sub>2</sub>
Current value	100 A, 130 A, 150 A
Wire material	ER70S-6 (Mild steel welding alloy)
Wire diameter	0.8 mm
Torch speed	0.5 m/minute



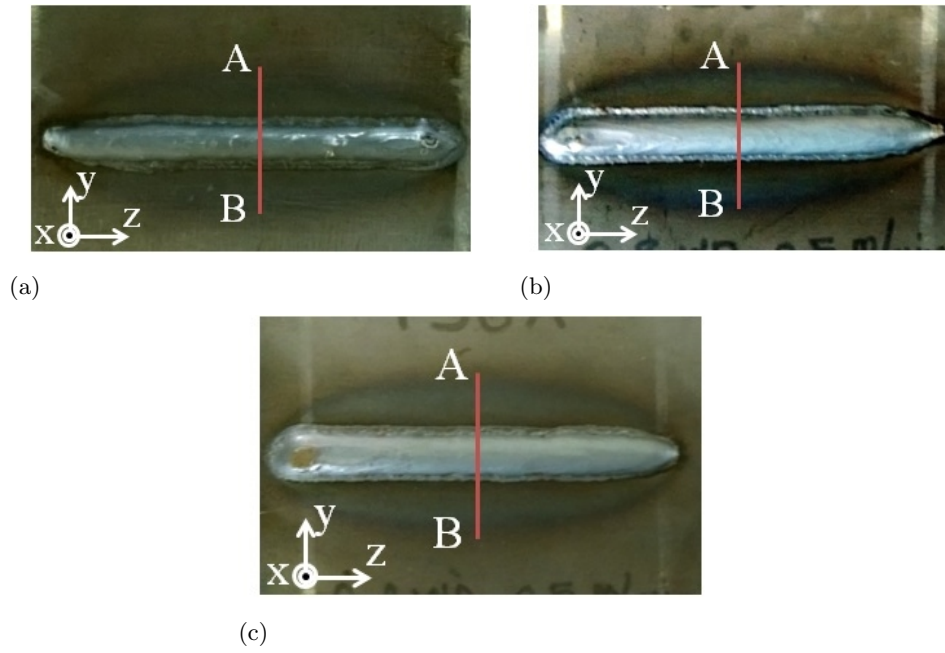


Figure 2.1: Top view of weld deposition made with different current ratings. (a) with 100 A (b) with 130 A and (c) with 150 A.

### 2.3 Micrographic Examination

In order to identify various zones of the weld, small rectangular sections are cut using EDM wire cut machine. The face parallel to the weld penetration is polished and etched using the solution made of 5% nitric acid and 95% ethanol. For examining the etched face, an optical microscope (Olympus STM6) with 5x, 10x and 50x zoom is used. An integrated three mega pixel camera is used for image grabbing. The zones corresponding to the weld inhomogeneities are visualized and from the calibrated table movements of the microscope, the coordinates of the boundary of various zones are measured. The fusion zone is characterized by the presence of dendritic structure and surrounding to FZ, heat affected zones contain higher grain size as compared to base material. In the present study the HAZs are divided into three sub zones, based on their average grain size. The coarse grain HAZ (HAZ1) is the region identified near to FZ having a larger grain size and further two fine sized grain HAZs (HAZ 2,3) and unaffected base metal (BM) are also identified. Micrographic view of different zones obtained using optical microscope are shown in Fig. (2.2,2.3). Schematic diagram showing the locations where the measurements are taken is depicted in Fig. 2.4(a). Strain data corresponding to these zones are obtained from DIC technique and the methodology is explained in section (2.5.2).

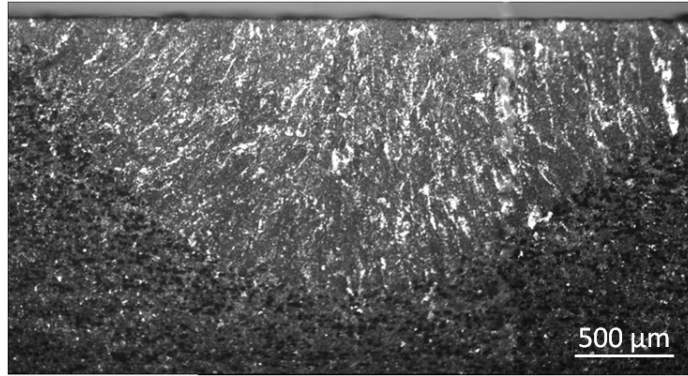


Figure 2.2: Optical microscopic image of an etched sample of 150 A weld at 5x magnification.

## 2.4 Vickers Microhardness Testing

Microhardness examination of the weld is a common and widely accepted method for examining the variation of hardness across it. The measured hardness values cannot be directly linked to the constitutive parameters, but they are helpful in the following aspects. Hardness values can be used as a check for the formation of microstructures having low ductility and toughness which are prone to cracking. In steel pipeline welds the formation of martensite in the HAZ results in crack prone zone formation. So for this type of weld a maximum value for the hardness can be used as a check for weld integrity and it could be related to the susceptibility of the material towards some kind of stress corrosion [2]. In this study, Vickers microhardness test (using Dura Scan make microhardness testing set up) is performed along the thickness and transverse direction of the weld. All the tests are done on a small rectangular specimen used for zone identification. In order to produce further smooth surface for microhardness testing all the specimen faces are polished to one micron level using diamond powder paste. A load of 300 grams ( $HV_{0.3}$ ) is applied and the hardness values are obtained at an interval of 0.25 mm length. Fig. 2.4(b) shows the direction in the form of lines along which the microhardness values are evaluated and the obtained results are discussed in subsection (2.6.2).

## 2.5 Constitutive Parameter Estimation

In this section the methodology adopted to identify the constitutive parameters of various zones of the weld using DIC is described.

### 2.5.1 Specimen dimensions and Tensile Testing

Transverse weld tensile specimens are made from the weld deposited sheets using EDM wire cut. Fig. 3.1 shows the orientation of the dog bone sample over the weld deposited mild steel sheet. Dimensions of the specimen is in accordance with the sub-sized specimen

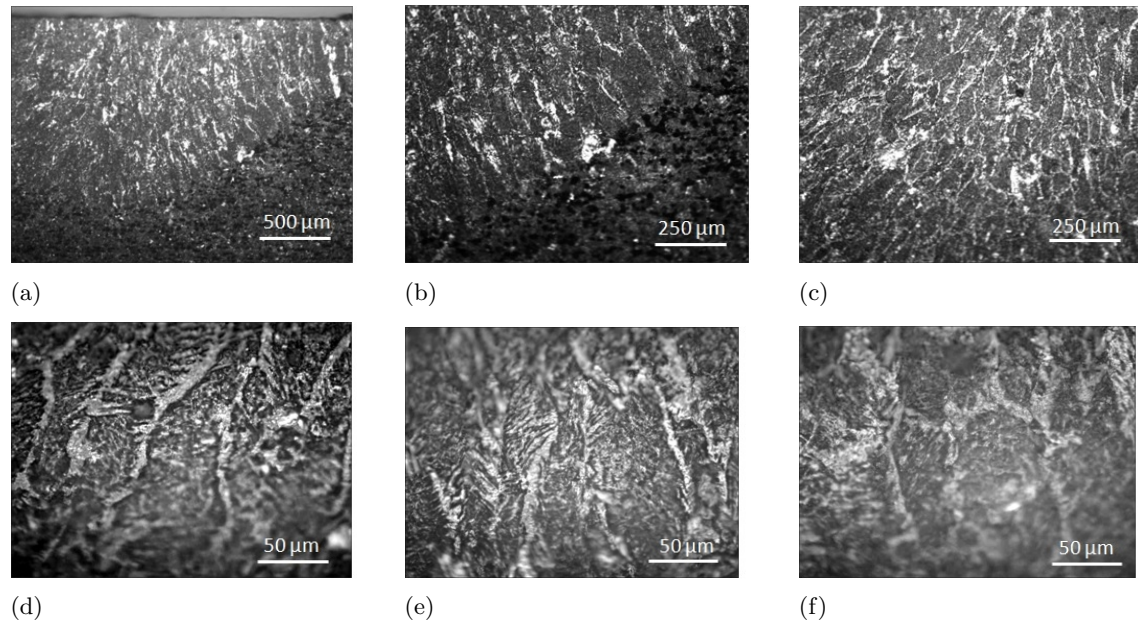


Figure 2.3: Optical microscope images of etched samples at various magnifications. (a) fusion zone at 5x zoom. dendrite structure can be identified. (b),(c) fusion zone at 10x zoom. (d),(e) fusion zone with dendrite structures at 50x zoom. (f) Heat affected zone at 50x zoom. All these images belong to weld zone of 150 A specimen.

dimensions given in reference [42] and refer Fig. 3.2(b) for the specimen dimensions used in this study. Prior to making tensile samples, the projected weld depositions are removed using rotary surface grinder for making the cross-section uniform throughout the gauge section. Refer Fig. 2.6 for the tensile samples painted with and without speckle patterns. In order to compare the properties of different zones with that of the base material, virgin tensile samples are also prepared. Experiments are performed under static loading using a computer controlled MTS Landmark<sup>®</sup> servo hydraulic cyclic testing machine of 100 kN capacity having a data acquisition system. Self adjusting hydraulic test fixtures are used to grip the specimens. The specimens are tested at a speed of 1 mm per minute. The DIC system consists of a 8-bit Grasshopper<sup>®</sup> CCD Camera (POINTGREY- GRAS-50S5M-C) having a spatial resolution of 2448 x 2048 pixels fitted with Tamron<sup>®</sup> zoom lens of 185 mm focal length. In the present study the images are recorded at a rate of 300 images per minute. Load value for every image being captured is recorded using a separate data acquisition system. An extensometer is also used for capturing the gauge section strain as they are the classical method of measuring strain in a tensile test. The experimental setup used for this study is shown in Fig. 3.6(a).

### 2.5.2 Zone Identification

This section explains the methodology used to identify different weld zones such as fusion and heat affected zones from the post processed DIC images. It is important to identify the

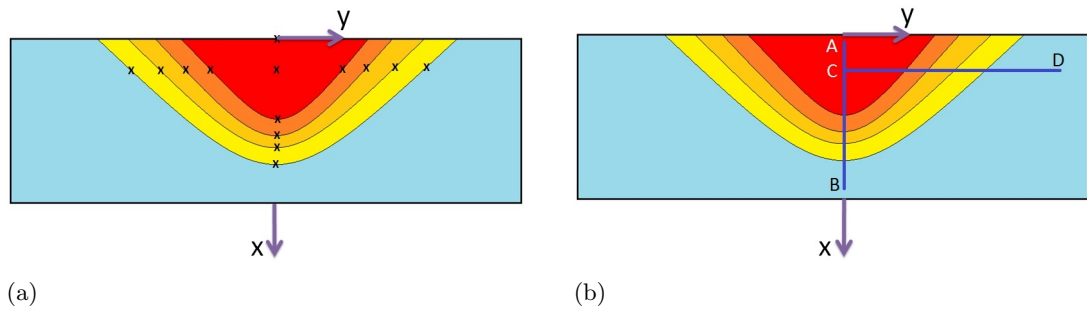


Figure 2.4: Figure showing measurement locations. (a) Coordinates of the points marked 'X' are measured using Optical microscope. (b) Vickers micro hardness testing carried out in the thickness (line AB) and length direction (line CD), where C is the center of fusion zone.

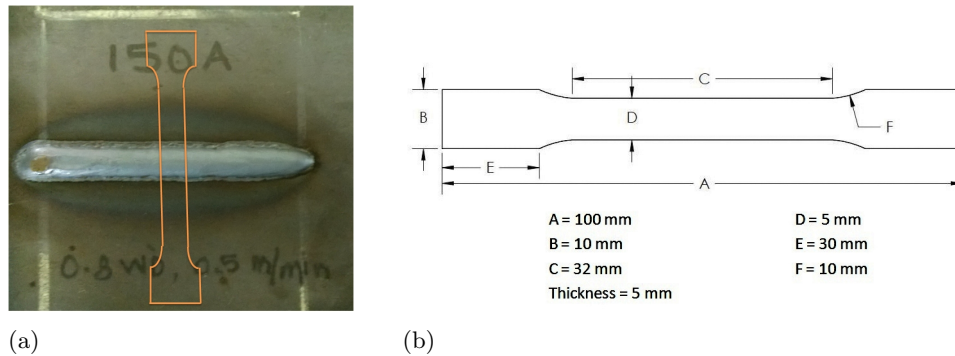


Figure 2.5: Specimen geometries used for characterisation (a) orientation of the specimen with respect to the weld (b) dimension of the tensile specimen.

pixels of the image belonging to different weld zone for determining the local constitutive parameters. If the pixels of various zones are identified from the image being captured during the test, then the strain values of the respective zones at various load levels could be traced and extracted. Since the specimens are painted with speckle patterns it becomes impossible to directly identify the zones. An approximate identification could be done looking at the micrographic image. In this study a strain based method is used for accurate identification of various zones. Post processed images show strain variation across weld zones. The longitudinal strain contours obtained at different load levels using DIC are shown in Fig. 2.8. The variation is clearly visible in the strain states falling in the plastic deformation region. In all the experiments the fusion zone is experiencing the least strain and gradually increases from coarse grain HAZ towards base material. Fig. 2.9(a), shows the typical longitudinal strain distribution over a weld deposited specimen under plastic deformation. The strain contours in the Fig. 2.9(a) are not directly related to various zones but it is evident from the strain distribution that there is a variation in strain level across the weld. This property is used for the zone identification and it is explained below.

A line is drawn along the thickness direction as shown in Fig. 2.9(a). Strain values

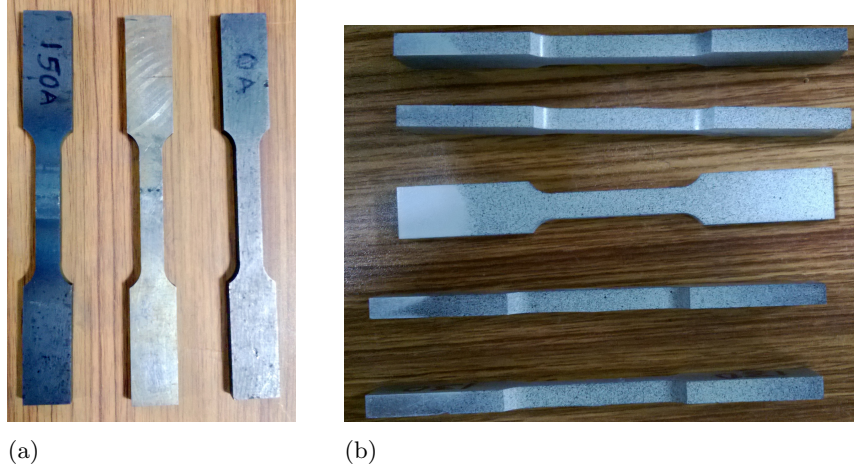


Figure 2.6: Weld specimens used for testing (a) specimens without speckle pattern (b) specimens with speckle pattern.

and corresponding coordinates of the points lying on that line segment is collected using image correlation software (Vic-2D). The  $x$  coordinates of the extracted data is nothing but the distance from the weld surface. A MATLAB<sup>®</sup> program is written for identifying the pixels of the image belonging to different weld zones. The inputs to the program are the coordinates of the boundary of each zone measured using an optical microscope as described in section (2.3) and longitudinal strain ( $\varepsilon_{yy}$ ) obtained from DIC. Initially the program will plot the longitudinal strain versus distance over the weld surface and it is subdivided in to various zones using the coordinate information obtained from the micrographic examination. Fig. 2.9(b) shows the subdivided plot and it is clear that there is a continuous increase in longitudinal strain from the fusion zone towards base material. Highest strain value in FZ is identified and using the DIC pixel data and image processing toolbox of MATLAB<sup>®</sup> the pixels corresponding to those strain levels equal to or less than the highest strain level are identified for the fusion zone and highlighted on the image. In the next step the pixels corresponding to the strain levels more than the maximum strain value of fusion zone and equal to or less than the maximum strain value identified for coarse grain HAZ are collected and highlighted on the image. The same exercise is continued till all the zones are identified. Fig. 2.10 shows the images with identified pixels highlighted for respective zones. The same routine is used for identifying the zone wise pixel information for the welds made with different current ratings.

### 2.5.3 Constitutive Models and Parameter Estimation

In this section the constitutive models and the methodology used for identifying the constitutive parameters are discussed. The elastic constitutive parameters estimated are the Young's modulus ( $E$ ) and Poisson's ratio ( $\nu$ ). Hollomon's power law [43] is used to characterise the plastic deformation and the strain hardening behaviour. The relations between

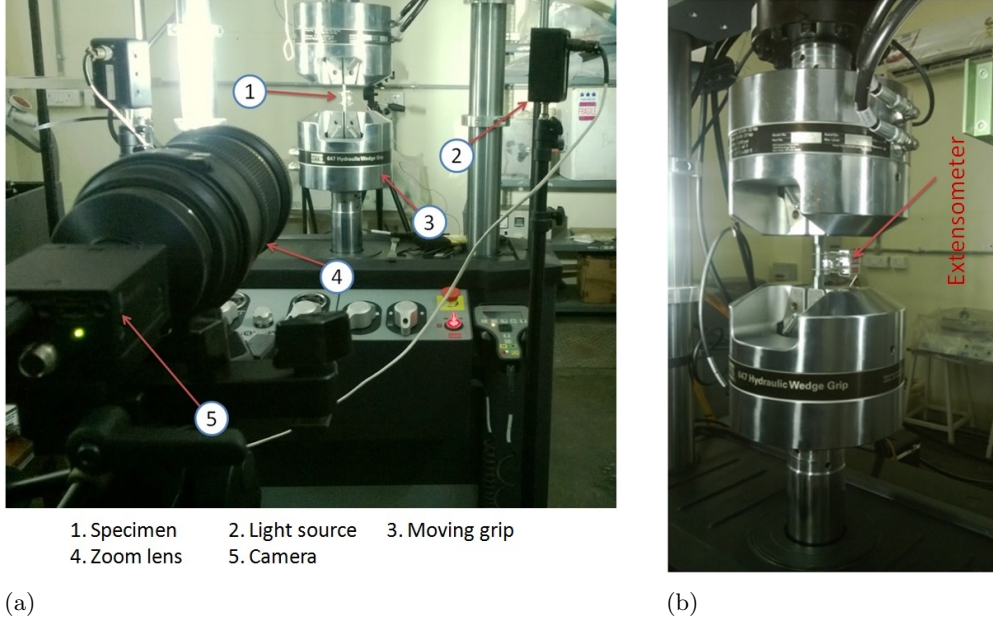


Figure 2.7: Experimental set up involving DIC (a) overall set up (b) zoomed view of the gripped specimen with extensometer attached.

the parameters under investigation are given in Eq. (4.1), where  $\varepsilon_{yy}$  is the longitudinal strain,  $\sigma_{yy}$  is the corresponding longitudinal stress,  $\sigma_{pl}$  is the stress at proportionality limit,  $\sigma_{ys}$  is the yield stress which is 0.2% proof stress,  $K$  is the strength coefficient and  $n$  is the strain hardening exponent.

$$\sigma_{yy} = \begin{cases} E\varepsilon_{yy}, & \forall \sigma_{yy} < \sigma_{pl} \\ K\varepsilon_{yy}^n, & \forall \sigma_{yy} > \sigma_{ys} \end{cases} \quad (2.1)$$

The known parameters which are directly obtained from the experiments are  $\sigma_{yy}$  and  $\varepsilon_{yy}$ . Since isostress assumption is applied, the longitudinal stress ( $\sigma_{yy}$ ) is nothing but the ratio of load value obtained from the load cell to the cross-sectional area of gauge section. The longitudinal strain ( $\varepsilon_{yy}$ ) values are designated in three ways, namely global, local and strain estimated by the extensometer (EM). The global strain is the average strain over the entire area of interest considered for image correlation. In this paper the term 'global' is used for indicating the average property obtained using DIC. This area will include fusion zone, various heat affected zones and some portion of the base material. Local strain is the average strain value of individual zones of the weld obtained using DIC. For each load levels, both longitudinal strain ( $\varepsilon_{yy}$ ) and lateral strain ( $\varepsilon_{xx}$ ) of each zone are extracted. Extensometer is also connected across the weld zone and for all the experiments. It's removal point is set as 0.2% strain. The strain value from extensometer are recorded and are compared with global strain value obtained from DIC. The unknown parameters are extracted from the stress verses strain curve and fitting it using method of least squares. A straight line is fitted

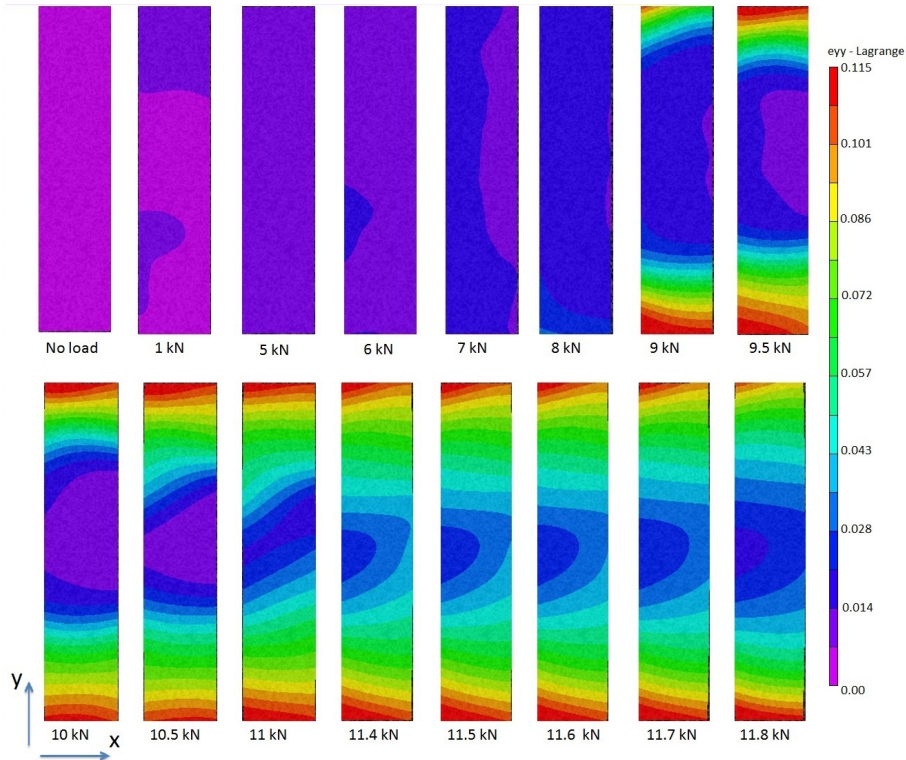


Figure 2.8: Longitudinal strain ( $\varepsilon_{yy}$ ) obtained using DIC at different load levels over the weld zone for the 130 A specimen.

to the linear elastic data and its slope corresponds to the Young's modulus. Hollomon's power law is fitted to the nonlinear data. Any discontinuity and disturbances recorded during the transition of elastic to plastic deformation such as unstable yielding like upper and lower yield points are omitted while fitting the curve. Stress versus strain curves are plotted for global, local and extensometer strain data. The local stress-strain curves of each zone is the local response of that particular zone and global stress-strain curve will provide the details on the average response of the area under study.

Data extraction, curve plotting and parameter identifications are automated by an algorithm written in MATLAB<sup>®</sup> software. The procedure adopted for finding out the strength coefficient and strain hardening exponent is in line with [44, 45]. Poisson's ratio extraction is done in accordance with the method described in [46]. The entire process is summarised in Fig. 2.11.

## 2.6 Results and Discussions

Observations and results of the micrographic examination, Vicker's microhardness measurement and constitutive parameter extraction are discussed in detail in the following subsections.

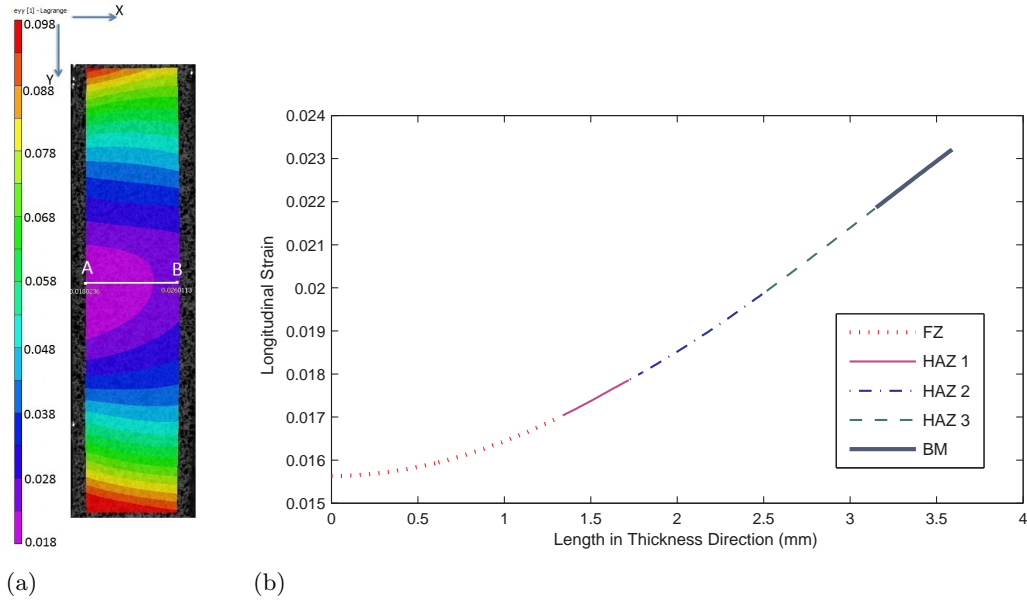


Figure 2.9: Zone identification using strain distribution. (a) longitudinal strain ( $\varepsilon_{yy}$ ) contours during the plastic deformation of a 130 A specimen estimated at a load of 11.5 kN (b) ( $\varepsilon_{yy}$ ) distribution along the line shown in Fig. 2.9(a), divided into various zones.

### 2.6.1 Micrographic Examination

Objective and procedure of micrographic examination are elaborated in section (2.3). The measurements taken during the micrographic examinations has been utilized for zone identification as explained in section (2.5.2). In this section, the depth of weld penetration, that is the extent of the fusion zone along the thickness direction for three different welds produced with different current ratings are compared. The depth of penetration is obtained from the coordinates of the boundary of the fusion zone measured using optical microscope. The bar chart relating welding current and the depth of penetration is shown in Fig. 2.12. It is evident from the figure that the least depth of penetration is for the weld specimen with 100 A current and maximum for 130 A. The 150 A specimen has a penetration depth greater than that of 100 A but it is less than that of 130 A current weld. The reason for the least weld penetration of 100 A weld is because of the lesser amount of energy available for melting the base material compared to higher current value. The same phenomenon is not seen for 150 A weld, as it is lower than that of a 130 A weld. In twin wire welding, two arcs are present namely leading and trailing arc and they are responsible for the weld material deposition. The leading arc is responsible for creating an initial fusion zone and the trailing arc deposits more material and increase the depth of penetration. For the same torch speed the leading arc of 150 A welding deposits more material than the leading arc of 130 A current and the additional material lumped on the work piece makes difficult for the trailing arc to penetrate further into the base material resulting in decreased penetration depth.



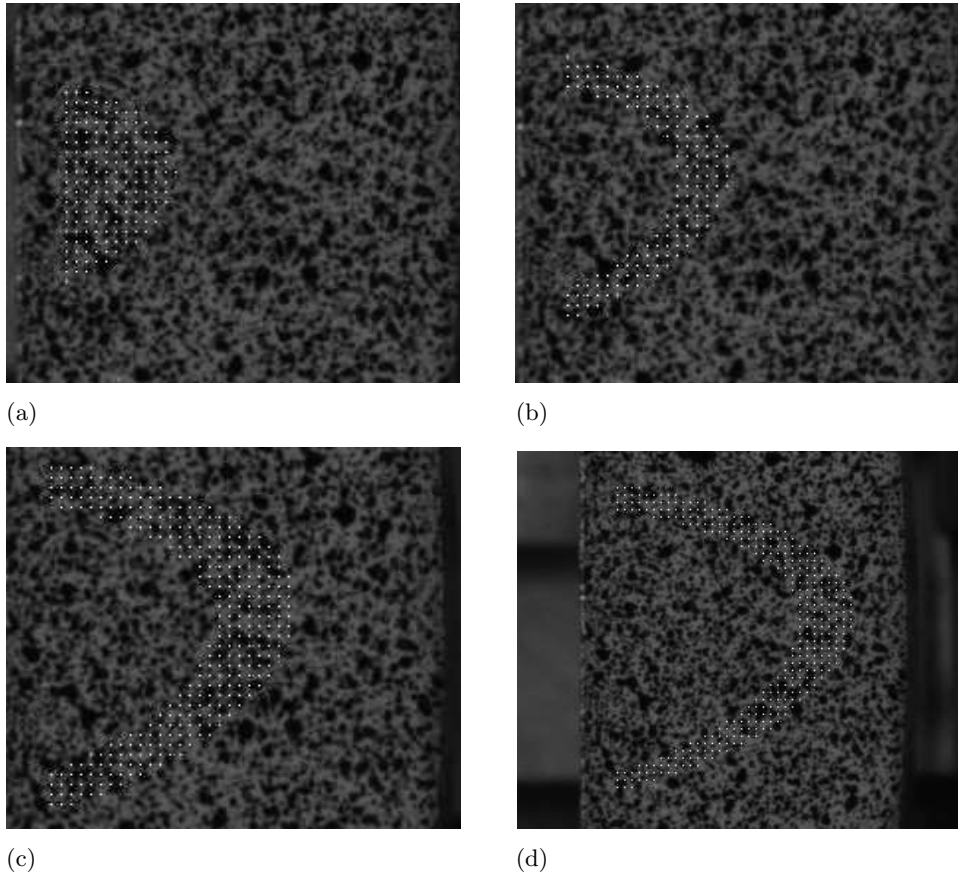


Figure 2.10: Images with pixels highlighted for various weld zones in 150 A specimen (a) fusion zone (b) coarse grain HAZ (c) fine grain HAZ 1 (d) fine grain HAZ 2. Pixels apart from these zones are considered as base metal.

## 2.6.2 Vicker's Microhardness Measurement

Hardness values ( $HV_{0.3}$ ) of the weldment and materials surrounding it is examined as explained in section (2.4) for different current rating specimens. Highest hardness value is recorded for the fusion zone and it decreases as one moves away from the fusion zone. The least value is recorded for the base material. Fig. 2.13 shows the plot relating the hardness values and measurement locations. The highest recorded hardness value is 233 ( $HV_{0.3}$ ) for the fusion zone of 100 A weld and lowest is for the base material whose value is 149 ( $HV_{0.3}$ ). The maximum hardness value is of fusion zone and its percentage deviation from the base material hardness values are tabulated in Table (2.3). The higher hardness value of fusion zone is primarily due to the fact that the fusion zone and HAZs are strain hardened upon plastic deformation and become more brittle.

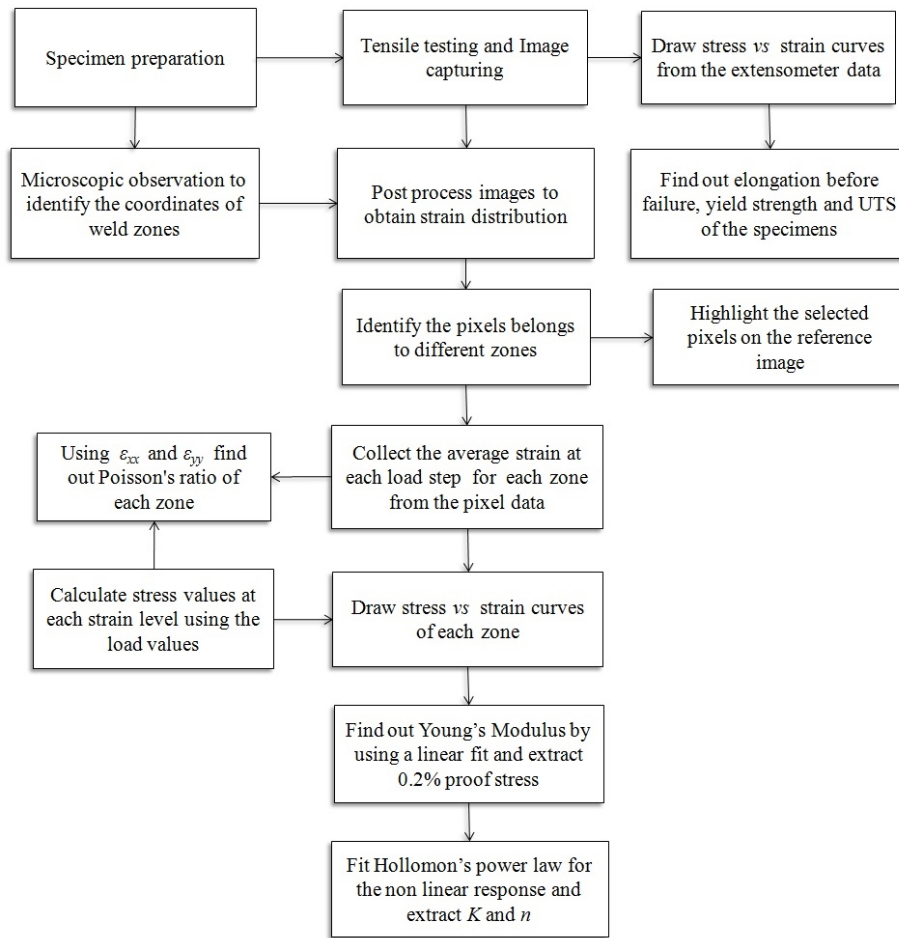


Figure 2.11: Processes involved in parameter extraction for local weld zones involving DIC

### 2.6.3 Constitutive Parameters

Constitutive parameters and the methodology used for extracting them has been discussed in section (2.5.3). Direct findings from the tensile tests are the failure location and total elongation before failure. The tensile test revealed that the samples with weld deposition broke at a location away from the welds nearer to the gripping region, (see Fig. 4.3). So it can be interpreted that the weld depositions are having higher strength properties as compared to base material. Elongation data are obtained directly from the MTS machine and the corresponding stress-strain plots are shown in Fig. 2.15. Predominant yielding seen in the case of virgin sample whereas it is absent in case of welded samples. As compared to the virgin sample a 39% decrease in elongation at ultimate tensile stress (UTS) is observed for 100 A specimen and 44% for 130 A and 150 A specimens (see Table 2.4). It can be interpreted from the elongation results that there is a clear increase in specimen stiffness in the presence of weld. UTS value of all samples are found to be more or less the same. Exact values of UTS and their deviation from the virgin sample is tabulated in Table 2.4. The reason for the sameness of the UTS is due to the fact that the region where the

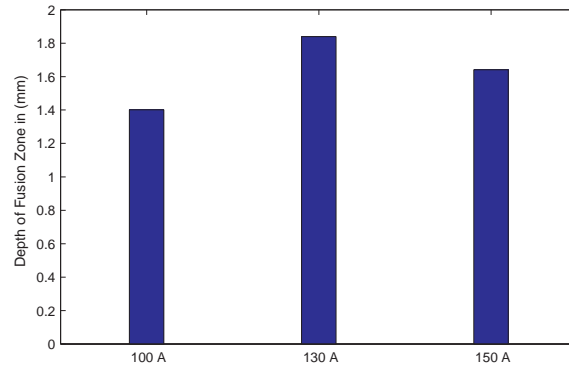


Figure 2.12: Depth of weld penetration for different current ratings.

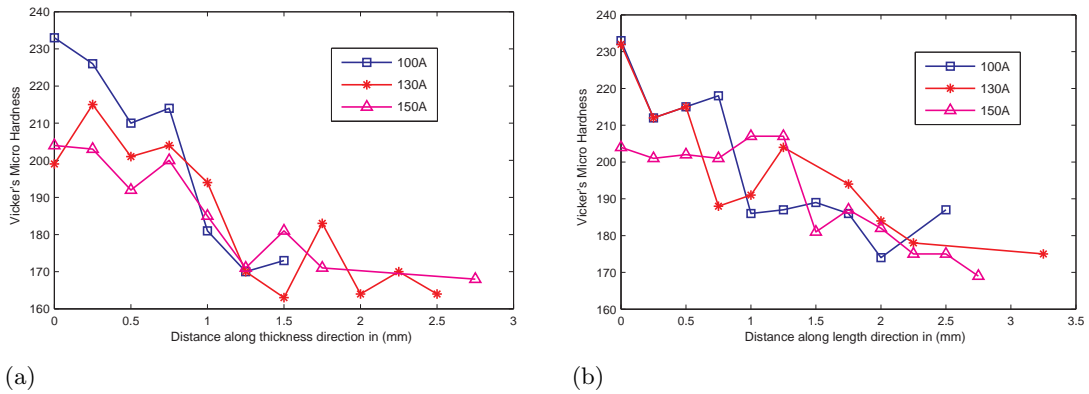


Figure 2.13: Vickers micro hardness measurement across weld zone. (a) Variation of HV<sub>0.3</sub> in thickness direction. (b) Variation of HV<sub>0.3</sub> along longitudinal direction.

failure occurred belong to the base material and since the base material is having the same properties as that of the virgin sample therefore the UTS value remained same irrespective of the weld. Above analysis is done using the data obtained from the extensometer which is an average response of the material. It is not possible to extract the variability of parameters and local responses of each weld zone from the extensometer data. Yield stress obtained from extensometer reading is also compared with the DIC and virgin sample results (See Fig. 2.17) and are in good coherence. The term 'Global' represents the average value of strain obtained from DIC over the entire area. There is difference in the yield stress value from extensometer reading and global DIC because the extensometer legs are resting on the base material and most of the material in between the extensometer legs comprises of base material than HAZs. So, the yield stress predicted by extensometer falls close to yield stress of the base material. Zone identification and zone wise strain data are materialised using the whole field strain data from DIC coupled with MATLAB<sup>®</sup>, as explained previously in section (2.5.3). The local stress-strain plots of the corresponding zones obtained using DIC are shown in Fig. 2.16. The main observation from the plot is that fusion zone exhibits a higher yield stress as compared to other zones. Virgin sample offered a yield stress of

Table 2.3: Percentage variation between maximum and base material hardness for specimens with different current ratings.

Current	Highest recorded HV <sub>0.3</sub>	% Increase from base metal HV <sub>0.3</sub>
100 A	233	56.37
130 A	232	55.70
150 A	207	38.92

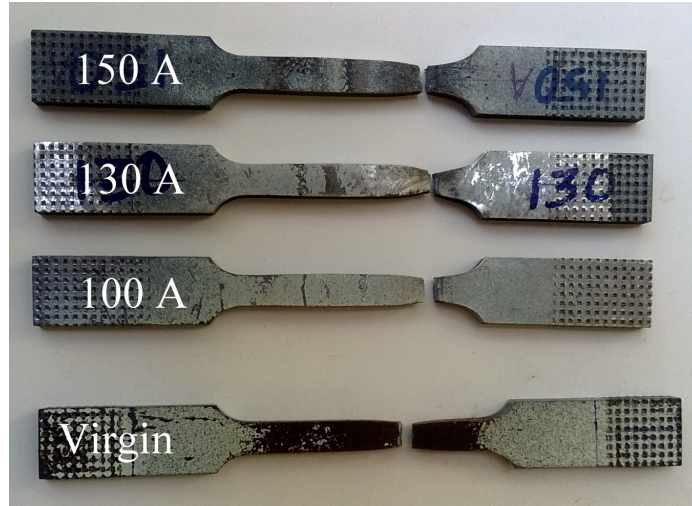


Figure 2.14: Fractured specimens after tensile testing. Current rating used for welding is mentioned on the samples.

301 MPa. Variation of yield stress of different zones for different weld current is plotted in Fig. 2.18(a) and the percentage deviation of zone wise yield stress from the virgin sample is given in Table 2.5.

Maximum reported value of the average longitudinal strain ( $\varepsilon_{yy}^{max}$ ) experienced by each zone are compared and it is found that the fusion zone is least strained. Fig. 2.18(b) shows the plot of maximum average longitudinal strain of different zones for different weld current. As weld current increases  $\varepsilon_{yy}^{max}$  experienced by the base material also increases. This behaviour is due to the presence of a larger and strain hardened fusion zone cum HAZs associated with an increase in weld current. These zones will undergo more strain hardening resulting in lesser contribution towards energy dissipation. So there is a decrease in the ductility of fusion zone as well as HAZs compared to the base material. Young's modulus, strength coefficient and strain hardening exponents are extracted by fitting curves on the stress-strain plot. Fig. 2.19 shows the fitted curves for the fusion zone of specimen welded with 130 A current. Same methodology is adopted for all other specimens over various weld zones.

The Young's modulus obtained for different zones revealed that there is a decrease in  $E$  value from base material towards fusion zone and the global value of Young's modulus

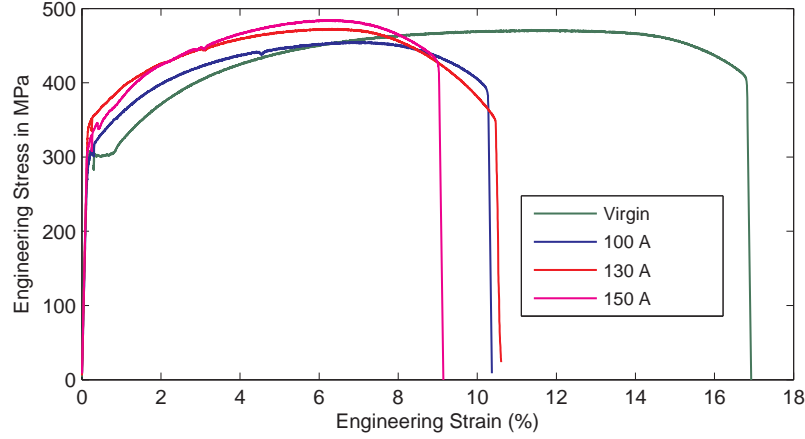


Figure 2.15: Stress - strain curves obtained from the extensometer reading.

Table 2.4: Obtained values of elongation and ultimate tensile strength for different weld specimens.

Current	Elongation in mm at UTS	UTS in (MPa)	% Change of UTS from virgin sample
Virgin sample	6.700	471	0
100A	4.275	455	-3.4
130A	3.695	472	0.3
150A	3.749	484	2.8

is also on the lower side as compared to virgin sample. This difference is in line with the observation reported in [33]. Yilbas *et al.* [47] attributed this variation to the size and cooling rate of the fusion zone and HAZs. The cooling of the molten metal in the fusion zone at atmospheric temperature results in the increase of ductility. The improved ductility causes more deformations during elastic deformation and results in lower Young's modulus. In the plastic deformation region the same trend is not seen because of the dominant strain hardening effect which results in the reduction of ductility. This variation can also be due to the residual stresses which are generated while welding and non-uniform distribution of fusion and heat affected zones. It is clear from the literature [48–50] that the fusion zone of an arc welded butt joint experiences high tensile residual stresses and it decreases gradually towards base material. Upon tensile loading the residual tensile stress field of the fusion zone and HAZs will get added up to the applied stress and can alter the response of them compared to the base material and finally result in a lower Young's modulus.

Virgin samples exhibited  $E$  value of 217 MPa and both DIC and extensometer gives the same result. In Fig. 2.20  $E$  values based on extensometer readings are compared with DIC based estimation. The plots show that the extensometer gives the lowest value comparable to that of fusion zone and therefore one cannot consider the average response of the weldment for design purpose. Percentage variation of zone wise  $E$  value from the virgin

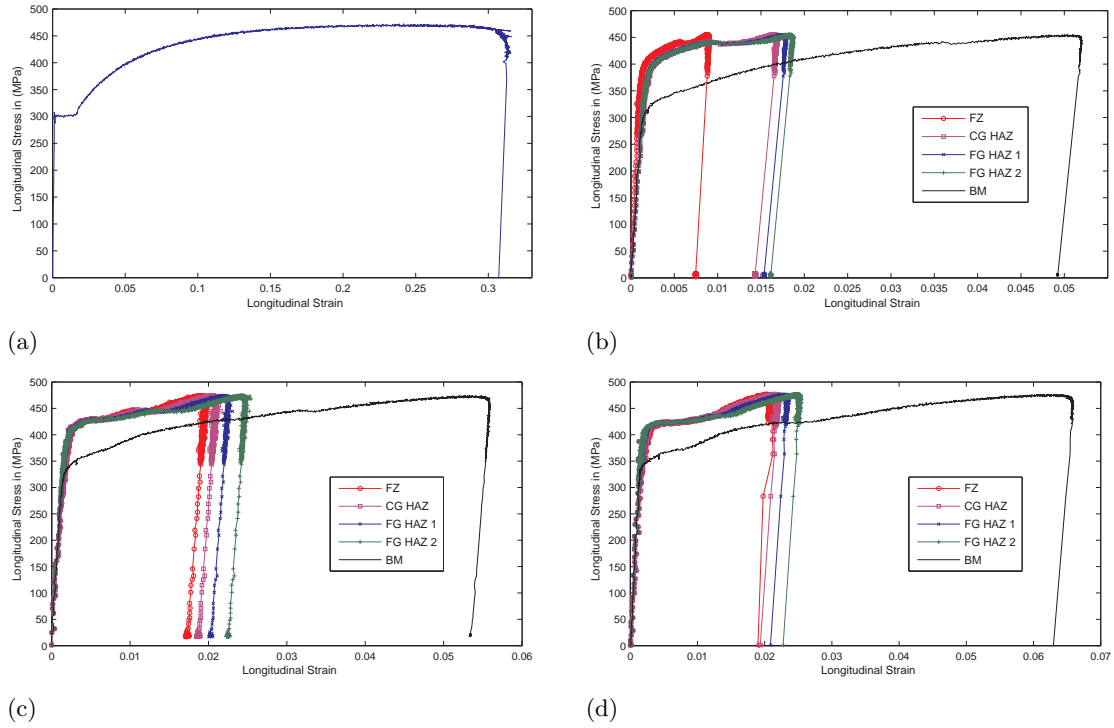


Figure 2.16: Stress-strain curve obtained using data from DIC technique (a) virgin sample (b) 100 A (c) 130 A (d) 150 A.

sample is given in Table 2.6. Variation of Young's modulus over weld zone for different specimens are plotted in Fig. 2.21. Strain hardening exponent ( $n$ ) is varying from zone to zone as shown in Fig. 2.22(a). Least and highest recorded value for  $n$  correspond to fine grain HAZs and base material respectively. As per the Hollomon's power law the strength of the material is inversely proportional to the magnitude of  $n$  [45], so it is clear from the Fig. 2.22(a) that the HAZs undergo a higher strain hardening followed by the fusion zone. The virgin sample reported a  $n$  value of 0.186. Variation of strength coefficient ( $K$ ) is shown in Fig. 2.22(b).

Poisson's ratio is obtained from estimating the ratio of transverse strain to longitudinal strain. Fig. 2.23 shows the variation of Poisson's ratio over various zone for different specimens. The virgin specimens reported a Poisson's ratio of 0.298 and the HAZs have higher Poisson's ratio value compared to other zones and the welding has increased the Poisson's ratio value. The constitutive parameters estimated zone wise, especially the yield strength and strain hardening exponent is in line with the micro hardness values investigated across the weld zone. The fusion zone and the HAZs offered a higher hardness, higher yield stress and higher strain hardening effect compared to the base material.

Table 2.5: Percentage increase of yield stress in comparison with virgin sample.

	100A	130A	150A
FZ	41.65	40.84	39.48
HAZ 1	38.42	41.42	40.24
HAZ 2	38.17	41.13	40.24
HAZ 3	37.96	40.92	40.07
BM	11.73	17.83	18.88
Global	11.77	19.17	19.78

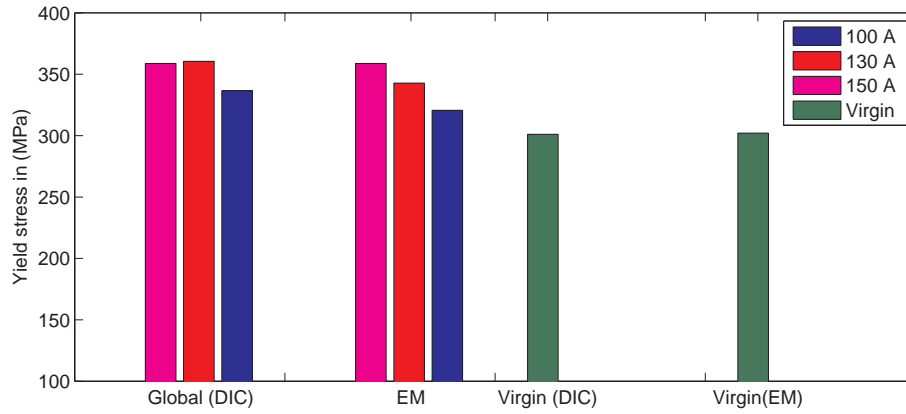


Figure 2.17: Comparison of yield stress estimated using extensometer (EM) readings and DIC.

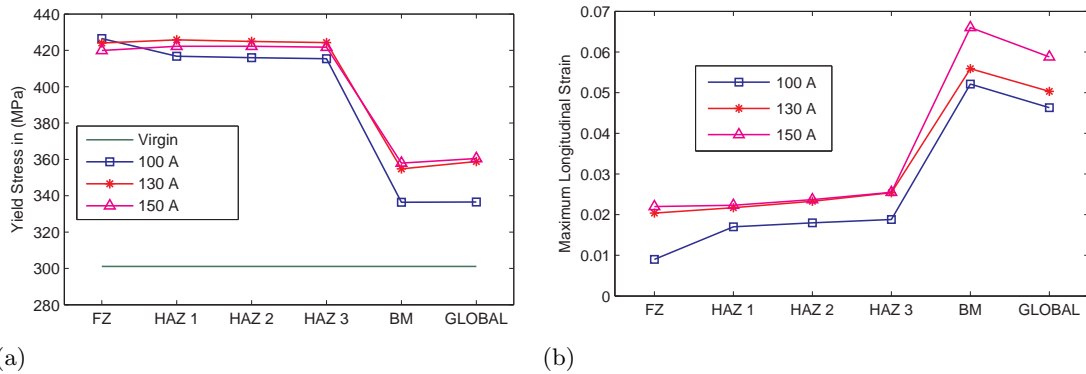


Figure 2.18: Yield stress and maximum strain variation across the weld zone (a) yield stress (b) maximum strain.

## 2.7 Closure

The identification and characterization of different thermally affected zones in a weld deposition have been successfully carried out using DIC technique. A new method is proposed for the identification of various zones using the strain data from DIC and boundary locations based on the micrographic examination. It is shown that the proposed method is useful in identifying various zones of weld with reasonable accuracy. The identification of zones has

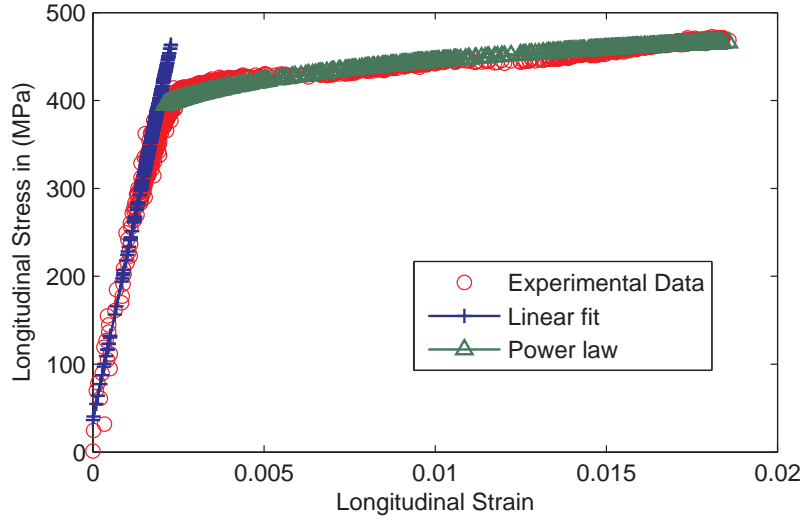


Figure 2.19: Linear and non linear curves fitted on experimental data for parameter extraction corresponding to the fusion zone of 130 A specimen.

Table 2.6: Percentage variation of Young's modulus in comparison with virgin sample.

	100A	130A	150A
FZ	-8.61	-12.97	-7.89
HAZ 1	-5.53	-10.16	-5.04
HAZ 2	-6.03	-7.38	-4.81
HAZ 3	-6.04	-3.76	-4.46
BM	-1.75	-2.42	-2.90
Global	-1.60	-2.34	-1.86

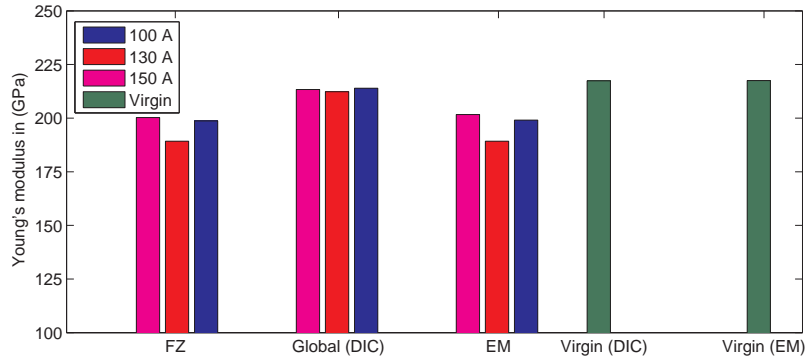


Figure 2.20: Comparison of Young's modulus estimated using extensometer (EM) readings and DIC

helped us in tracing the deformation pattern and thereby extracting zone wise strain values for different load levels. Microhardness measurements across the weldment indicated the variation of properties zone wise and the extracted constitutive parameters also followed the same thereby reassuring the accuracy of the proposed method. A major advantage of



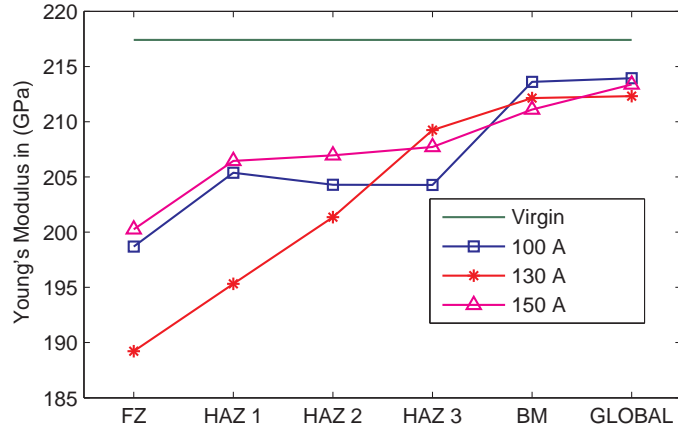


Figure 2.21: Variation of Young's modulus across weld zones for specimens with different current ratings.

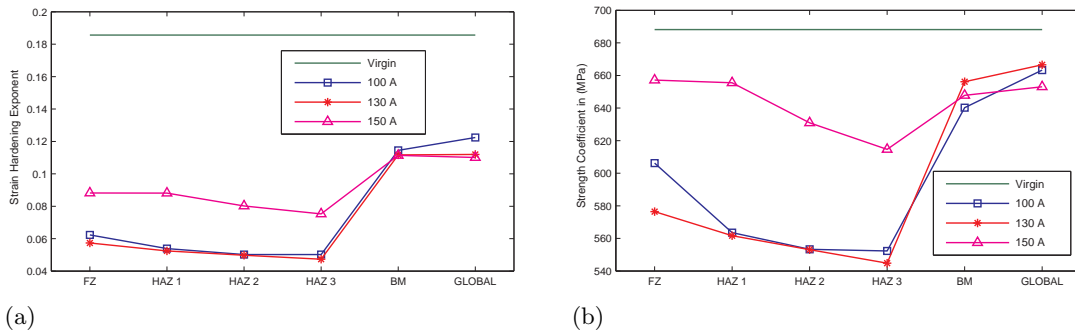


Figure 2.22: Variation of strain hardening exponent and strength coefficient across weld zones for specimens with different current ratings (a) strain hardening exponent (b) strength coefficient.

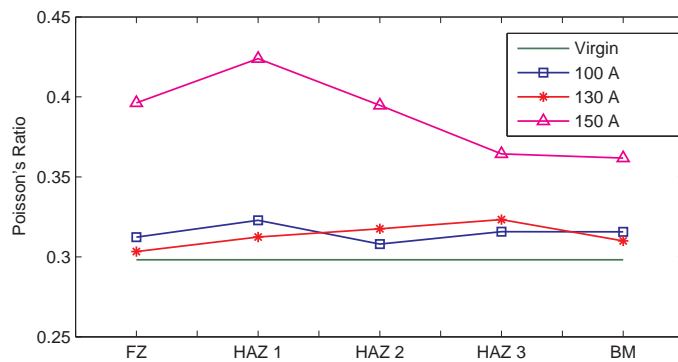


Figure 2.23: Variation of Poisson's ratio across weld zone for specimens with different current ratings.

the methodology adopted for this study is the extraction of full range stress strain curves for each zone along with simultaneous extraction of global response. Full range stress strain curves are again utilized for the extraction of local constitutive parameters. As one gets

the stress-strain curves of various zones from a single test, the proposed method is easier than the classical miniature specimen testing and gives the true response of each zone in actual condition. Specimens with different current rated welds are also characterised for establishing the suitability of this method towards optimizing weld parameters.

Fusion zone has the highest yield value as well as strain hardening effect whereas the Young's modulus is the lowest as compared to other zones. All the weld zones have  $E$  values lower than that of virgin sample and they keep reducing from the base material towards fusion zone. In this study, a higher amperage weld gave properties closer to those of BM, but a detailed investigation on the influence of welding parameters on property distribution is required for an exact selection of optimized welding conditions. The location and yield stress of fracture zone is also an important factor in the assessment of weld quality as one needs the yield value corresponds to that zone for design estimate. This can be precisely estimated using the proposed approach. In the present study all the welded samples are fractured away from the weld region and the yield value estimate of the base material closer to weld zone of all the welded samples are on the lower side compared to other zones. This lower yield stress of base metal has resulted in the earlier yielding of it resulting in the fracture. The proposed methodology using DIC is found to be effective and accurate in predicting the local constitutive properties over the weld zone and its real utility will arise in case of weldment of thin sheets.

## Chapter 3

# Investigation of local zone wise elastic and plastic properties of electron beam welded Ti-6Al-4V alloy using DIC

### 3.1 Introduction

Titanium and its alloys are widely used in the manufacturing of critical engineering components because of their superior properties such as high strength to weight ratio, good corrosion resistance etc. Welding of titanium alloys are often considered as the important operation which dictates the quality of final product. Zone wise characterization of the weld is highly desirable for prediction of weld integrity and their by assuring the quality of final product. In this study the local zone wise elastic and plastic characterization of electron beam welded Ti-6Al-4V alloy is carried out using digital image correlation (DIC) technique. Microstructural variations obtained from micrographic examination is utilized for identifying various weld zones such as fusion zone and heat affected zones. Using DIC technique zone wise full range stress-strain curves are extracted for each identified zones. Young's modulus, Poisson's ratio, yield stress, strength coefficient and strain hardening exponent are extracted from the zone wise stress-strain curves. Hollomon's power law is used as the material model for plastic zone characterization. From the zone wise parameters its observed that the fusion zone is having the least Young's modulus and exhibits higher Poisson's ratio, yield stress and strength coefficient. Base metal where the specimens failed has reported the lowest yield stress value. Heat affected zones have recorded a higher strain hardening exponent in comparison with other zones. Vicker's microhardness examination across the weld also followed the same trend as that of zone wise parameters extracted which reassured the accuracy of the implemented technique.

Nowadays, among various welding techniques electron beam welding (EBW) has gained popularity in many critical engineering applications. There are several advantages for EBW over conventional arc welding which make EBW a preferred welding technique in manufacture of critical components. The advantages are: High depth of penetration with high power density which help in avoiding multiple pass welds even for thicker work pieces, narrow HAZ and lesser distortion to the microstructure because of the lesser heat input during welding and its ability to weld reactive metals because of the requirement of vacuum helps the weld pool from reacting with atmospheric air and other impurities [2, 51]. Above advantages make EBW a suitable welding technique for welding titanium and its alloys [52].

Among the various alloys of titanium, Ti-6Al-4V, which is an  $\alpha$ - $\beta$  alloy of titanium, is the most industrially used one which accounts for almost 60% of the total titanium production. Also, this alloy has high strength to weight ratio compared to aerospace grade aluminium and steel alloys and good composite compatibility which makes this  $\alpha$ - $\beta$  alloy the most preferred titanium alloy for making various aerospace components [53]. Ti-6Al-4V has two allotropic phases of titanium which are hexagonally close pack structured  $\alpha$  phase and body centered cubic structured  $\beta$  phase. Also it contains 6% aluminium for  $\alpha$  stabilization and 4% vanadium for  $\beta$  stabilization [54]. This alloy is highly weldable because of the lower  $\beta$  stabilizing content [53]. There are many literature available on the micro structural studies, microhardness variation and global mechanical properties of titanium alloys welded using EBW [52, 54–57]. But a little studies are directed towards the zone wise local extraction of elastic and plastic properties of Ti-6Al-4V welded using EBW method.

## 3.2 Experimental Procedure

In this section various steps involved in the experiments carried out for zone wise local characterisation of weld such as welding, specimen preparation, micrographic examination, microhardness measurement, tensile testing and digital image correlation are elaborated in different subsections.

### 3.2.1 Welding and Specimen Preparation

Two Ti-6Al-4V alloy sheets of dimension 70 x 110 x 3 mm<sup>3</sup> are welded using EBW technique to form a 140 x 110 x 3 mm<sup>3</sup> welded sheet. Welding parameters used for creating the weld are given in Table 3.1. Transverse weld tensile specimens are made from the welded sheet using EDM wire cut. Fig. 3.1 shows the welded sheet and the orientation of tensile samples. The welded portion left out in between the tensile samples are used for micrographic examination. The weld reinforcement is not flushed in this study because its thickness is negligible in comparison to that of base metal thickness. Also, our aim is to get the properties of the weld as it is used in actual service conditions where the reinforcement is not machined. Area of interest (AOI), that is the plane where the surface strains are

measured, is the thickness face of the specimen. Tensile specimens showing AOI and the weld are depicted in Fig. 3.2(a). The dimensions of the specimen are in accordance with the sub-sized specimen dimensions given in reference [42] and refer Fig. 3.2(b) for the specimen dimensions used in this study.

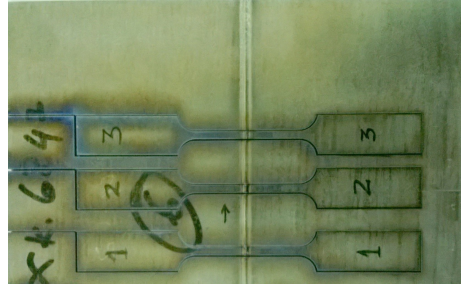
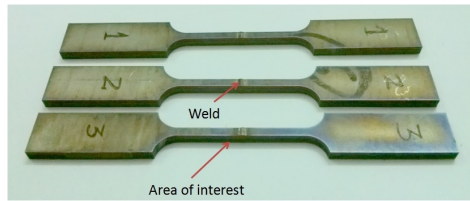
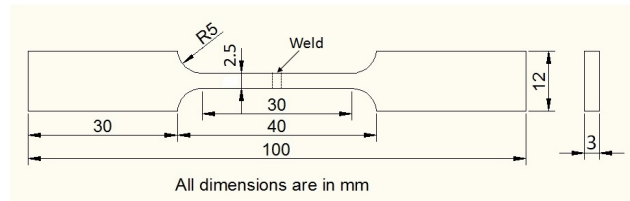


Figure 3.1: Welded sheet with tensile specimen orientation.



(a)



(b)

Figure 3.2: Tensile specimens with weld. (a) tensile specimens showing the AOI and weld (b) specimen dimensions.

Table 3.1: Details of welding methodology and parameters

Parameters	Values
Method	Electron beam welding
Electron accelerating voltage	140 kV
Beam Current	36 mA
Beam power	5.4 kW
Beam diameter	3 mm
Power density	713 W/mm <sup>2</sup>
Welding speed	2400 mm/min

### 3.2.2 Micrographic Examination

Thickness face of the weld is polished and then etched using Kroll's reagent for visualizing the microstructure of different zones of the weld. Microstructure variations are captured using an optical microscope (Leica DM 6000M) having calibrated scale. Fig. 3.3, 3.4 shows the micro structure across the weld at different magnification. The  $\alpha$  and  $\beta$  phases are clearly visible in the base material micrograph. The FZ is characterised with serrated and

rectangular plate shaped  $\alpha$  structure known as  $\alpha$  platelets. The reason for the formation of  $\alpha$  platelets in the FZ is the slow cooling rate of EBW. During a slow cooling process, the  $\beta$  phase undergoes a transition to plate like  $\alpha$  phase [58]. At higher cooling rates this  $\beta$  to  $\alpha$  platelet transformation does not take place instead of that martensitic transformation of  $\beta$  takes place and results in a more hardened zone. Apart from the microstructure assessment, the size of various weld zones are also measured using the micrographs. Width of FZ is found to be with in 1.3 to 1.5 mm and width of HAZ is lying in the range of 0.85 to 1 mm. This information is important for dividing the surface strain map into different zones for zone wise characterization of the weld.

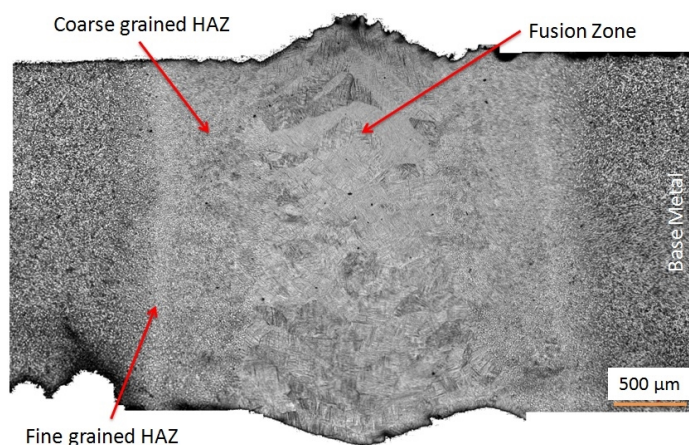


Figure 3.3: Microstructure of EBW at 5x magnification. Various weld zones are tagged in the figure.

### 3.2.3 Vicker's Microhardness Measurement

In order to find the variation of hardness across the weld Vicker's microhardness measurement is conducted across the weld on the specimen used for micrographic examination. The hardness values can be interpreted for finding crack prone zones which have low ductility and toughness. The variation in hardness will also give an indication about the trend of yield stress variation because a zone having higher yield stress is supposed to report a higher hardness value. In this study the Vicker's microhardness test (Using DuraScan microhardness tester) is performed along the line shown in the Fig. 3.5. A load of 300 grams ( $HV_{0.3}$ ) is applied and the hardness values are obtained at an interval of 0.2 mm length. Obtained hardness values and the discussion on the variation of hardness values are given in results and discussion section.

### 3.2.4 Tensile Testing and Digital Image Correlation

Transverse weld tensile samples are tested under static loading using MTS Landmark<sup>®</sup> servo hydraulic cyclic testing machine of 100 kN capacity. The system has got self ad-

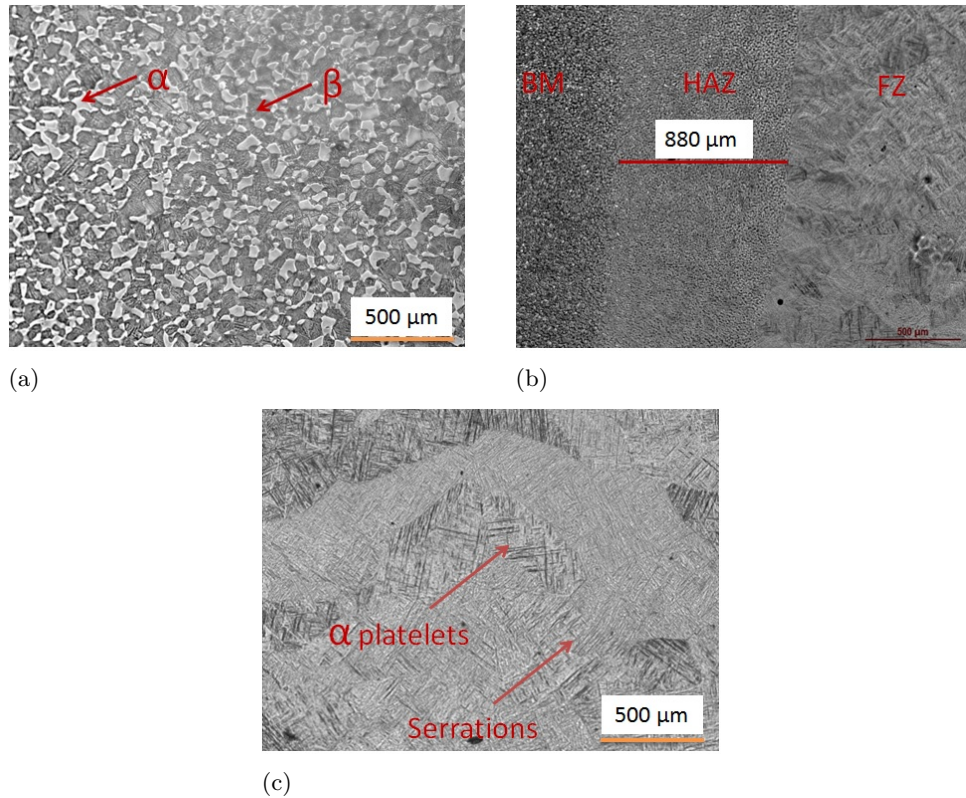


Figure 3.4: Zoomed view of the microstructure of different weld zones. (a) base metal at 20x magnification (b) FZ, HAZ and base metal at 5x magnification (c) FZ at 20x magnification.

justing hydraulic grips and an automated data acquisition system to record the load and displacement values. Specimens are tested at a speed of 0.5 mm per minute. In order to measure the surface strain distribution across the weld by using DIC, the thickness face of the specimen is painted with white paint and black dye is sprayed over it to make a random speckle pattern. A 2D DIC system is used in this study and it consists of an 8-bit Grasshopper<sup>®</sup> CCD Camera (POINTGREY- GRAS-50S5M-C) having a spatial resolution of 2448 x 2048 pixels fitted with Tamron<sup>®</sup> zoom lens of 185 mm focal length. In this study, 300 images are grabbed every minute. Load value for each image being captured is simultaneously recorded using a separate National instrument's data acquisition card interfacing MTS system with DIC hardware. More information on DIC is given in section 1.1.4. The experimental setup used in this study is shown in Figure 3.6(a) and speckled tensile sample loaded in the tensile testing setup is given in Fig. 3.6(b) An extensometer is also used for capturing the gauge section strain as they are the classical method of measuring strain in a tensile test.





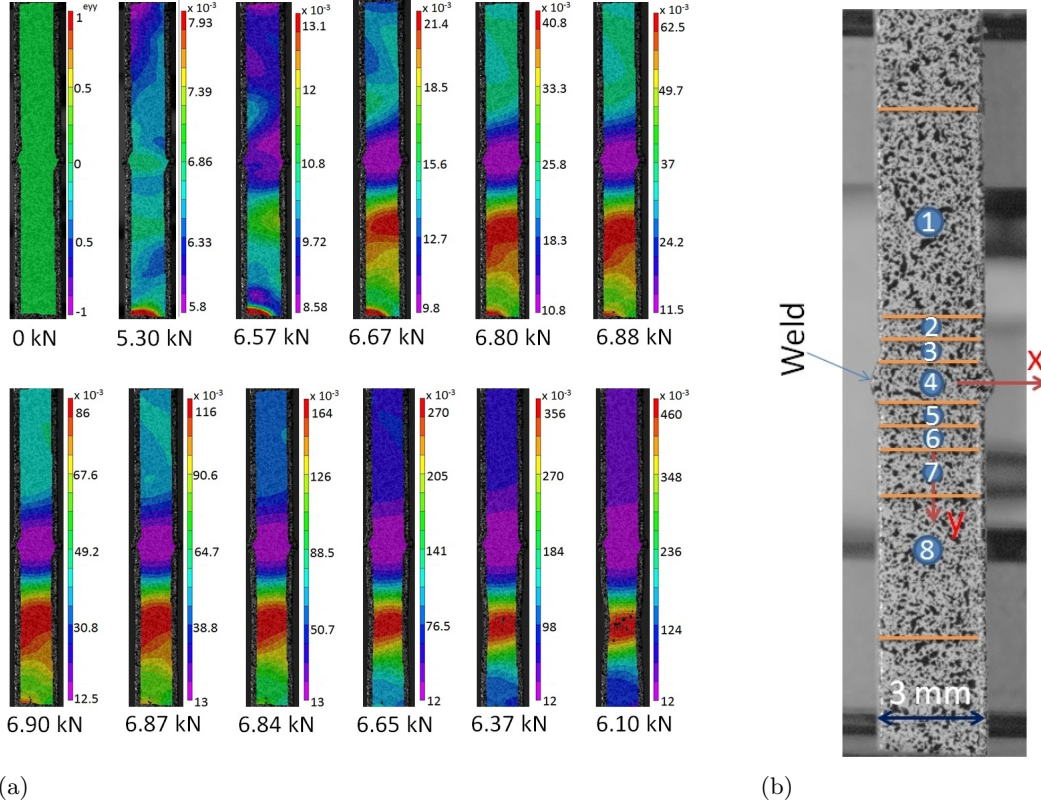


Figure 3.7: Strain evolution and divided AOI (a) Longitudinal strain distribution at various load levels (b) AOI divided into various zones

Table 3.2: Length of various zones which are identified in Fig. 3.7(b)

Zone index	1	2	3	4	5	6	7	8
Length in mm	7	0.8	0.8	1.35	0.8	0.8	2	5

zone that is the boundary between HAZ and BM, Zone '7' is the failure zone and '1' and '8' belongs to BM. Zone 7 is the location where the specimen necked and fractured which is identified to obtain the properties of failure zone.

Zone wise strain values are extracted from the strain distribution by writing a MATLAB<sup>®</sup> program which identifies the pixels belonging to various zones. The pixels are identified on the reference image by using image processing tool box of MATLAB<sup>®</sup> and the length information given in Table 3.2. In order to collect the zone wise strain information, the zone wise identified pixels are traced on each load steps and the average strain value of each zone are then returned to the system and stored.

### 3.3.2 Material Model

Young's modulus ( $E$ ) and Poisson's ratio ( $\nu$ ) are the unknown elastic parameters. In the plastic deformation region the sought parameters are strength coefficient ( $K$ ) and strain

hardening exponent ( $n$ ). Hollomon's power law is used as the material model for identifying plastic parameters. For each weld zone, these elastic and plastic parameters are extracted along with zone wise yield stress. The constitutive relation for the elastic and plastic parameters are given in Eq. 4.1. where  $\varepsilon_{yy}$  is the total longitudinal strain,  $\sigma_{yy}$  is the corresponding longitudinal stress,  $\sigma_{pl}$  is the stress at proportionality limit,  $\varepsilon_p$  is the longitudinal plastic strain,  $\sigma_{ys}$  is the yield stress which is 0.2% proof stress,  $K$  is the strength coefficient and  $n$  is the strain hardening exponent.

$$\sigma_{yy} = \begin{cases} E\varepsilon_{yy}, & \forall \sigma_{yy} < \sigma_{pl} \\ K\varepsilon_p^n, & \forall \sigma_{yy} > \sigma_{ys} \end{cases} \quad (3.1)$$

In the non linear plastic deformation zone ( $\sigma_{yy} > \sigma_{ys}$ ) the measured strain value is the sum of elastic and plastic strain. So in order to substitute the plastic strain in Eq. (4.1) the approximation given in Eq. 4.2 is used to decouple the plastic strain from the total strain.

$$\varepsilon_p \approx \varepsilon_{yy} - \left( \frac{\sigma_{yy}}{E} \right) \quad (3.2)$$

### 3.4 Solution Methodology

Unknown parameters are identified from the zone wise full range stress-strain curves. Zone wise strain data obtained using DIC technique is employed here to plot zone wise full range stress-strain curves. Uniform stress assumption is used for arriving at the stress values for plotting the curves. Young's modulus is identified by fitting a straight line on the elastic part of stress-strain curve and Poisson's ratio is identified as per the procedure described in ASTM E132-04 [46]. Yield stress is extracted by finding the intersection of 0.2% strain offset elastic curve with the experimental stress-strain curve. Plastic parameters are identified by fitting the Hollomon's power law by using method of least squares. Any discontinuity and disturbances recorded during the transition of elastic to plastic deformation such as unstable yielding like upper and lower yield points were omitted while fitting the curve. Apart from the local zone wise properties the global properties of the weld are identified from the average strain value of the entire AOI. These parameters are referred as 'global' in this study. Extensometer strain data is also utilised to get the elastic and plastic properties of the weld.

### 3.5 Results and Discussion

This section discuss in detail the results obtained from microhardness measurement and zone wise material parameters involving DIC technique.

### 3.5.1 Vicker's Microhardness

Vicker's microhardness value ( $HV_{0.3}$ ) measured along the line shown in Fig. 3.5 is depicted in Fig.3.8. The hardness variation is symmetric about the weld central line. It is clear from the figure that FZ is harder and the hardness value is reducing as one move away from the weld central line. The reason for the higher hardness of the FZ and HAZ compared the BM is due to the presence of  $\beta$  transferred  $\alpha$  platelets and small amount of hard martensitic  $\beta$  in the microstructure. These observations are in line with the microhardness results reported in Ref. [54, 59]. Maximum recorded hardness value is 379 ( $HV_{0.3}$ ) which belongs to the centre of FZ and the lowest recorded value is 336 ( $HV_{0.3}$ ) which belongs to the BM where the necking initiated during tensile testing..

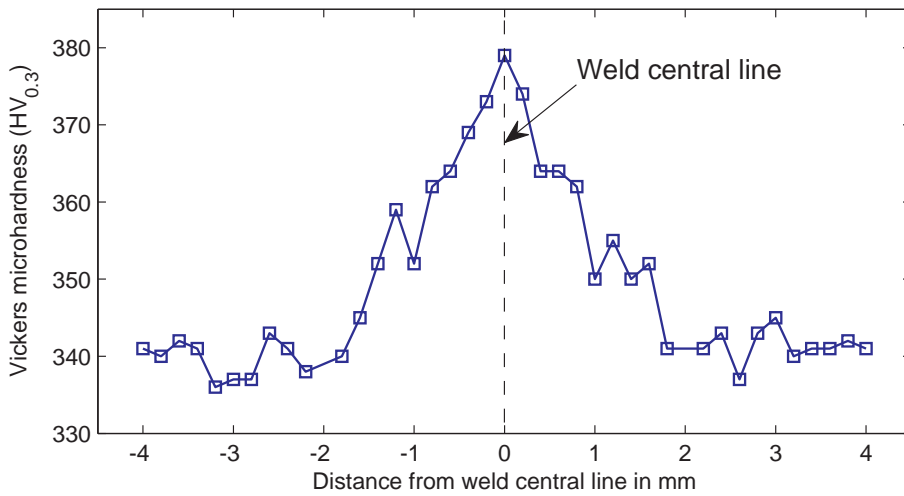


Figure 3.8: Vicker's microhardness variation across weld zones.

### 3.5.2 Tensile Test Results and Constitutive Parameters

Location where the failure initiate during tensile test is an important information for assessing the strength and quality of the weld. In this study all the three samples broke away from the weld central line at BM, in zone 7. Fig. 4.3 shows the fractured specimens. This conforms that the EBW used here for joining the base metal offers a higher strength than that of the base metal. Global constitutive properties are extracted from the stress-strain curves plotted using the strain information from extensometer and DIC. Fig. 3.10 shows the stress-strain diagrams obtained from both the technique. It is clear from the figure that the curves plotted using both the techniques are in very good agreement. The deviation of DIC curve from the extensometry curve at the failure initiation is due to the necking of the specimen which introduce out-of-the plane displacements like material shrinkage which in turn affect the image correlation and results in higher strain estimates. Constitutive parameters are extracted from these stress-strain curves using the methodology described

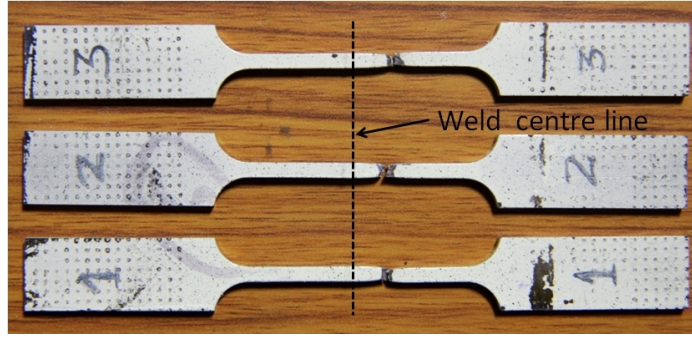


Figure 3.9: Fractured specimens after tensile testing.

in section 3.4 and values are given in Table 3.3. Apart from the parameters described in section 3.3.2, ultimate tensile strength ( $\sigma_{ut}$ ) and percentage elongation are also extracted from the global stress-strain curves and they are incorporated in Table 3.3. These global properties are in good agreement with the results reported by Wang *et al.* [54] where they have extracted  $\sigma_{ut}$ , and percentage elongation of Ti-6Al-4V welded using EBW technique.

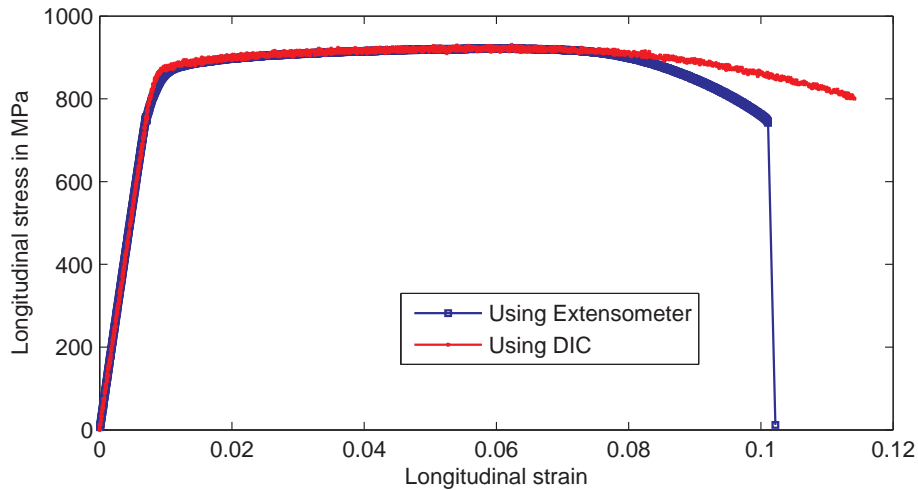


Figure 3.10: Global stress-strain curves obtained using extensometry and DIC technique.

Table 3.3: Global properties of the weld using Extensometry and DIC technique

Method	$E$ in GPa	$\sigma_{ys}$ in MPa	$\sigma_{ut}$ in MPa	$K$ in MPa	$n$	% elongation
Extensometry	108.64	859.28	922.65	986.14	0.021	9.7
DIC	106.55	877.20	930.27	971.25	0.017	-

In order to examine the variation of longitudinal strain the strain data across a line passing through the weld is collected and plotted for the strain distribution obtained for a load value of 6.76 kN which is given in Fig. 3.11. The observation from the figure are: FZ is experiencing least amount of strain and it increases as one move towards the BM and the

portion where the fracture occurred is experiencing higher strain compared to other zones of the specimen. It is clear from the figure that upon plastic deformation, FZ and HAZs undergo a higher strain hardening compared to BM and it is in line with the observations obtained from microhardness examination.

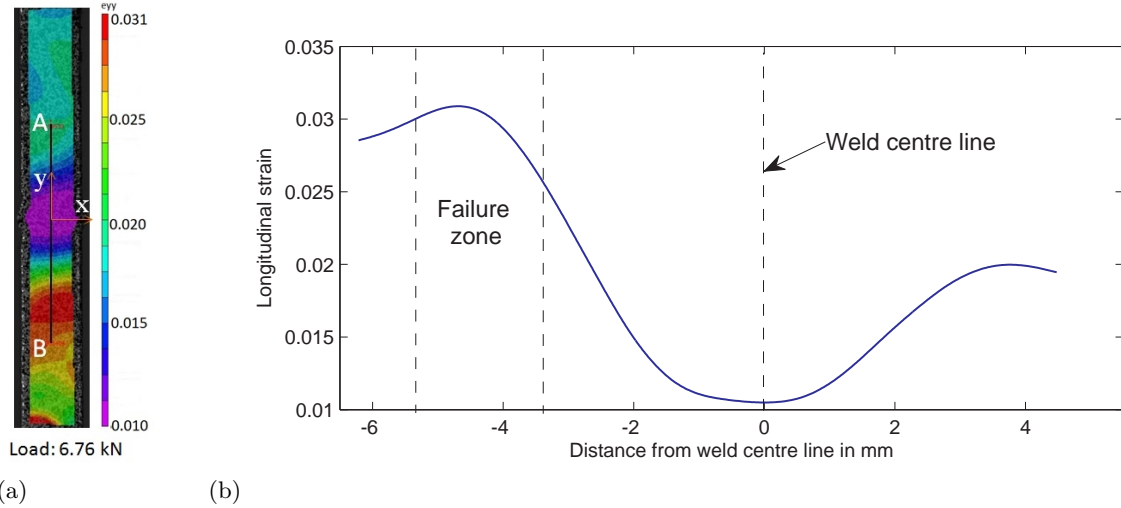


Figure 3.11: Variation of  $\epsilon_{yy}$  across the weld (a) figure showing line AB along which strain values are collected (b)  $\epsilon_{yy}$  variation along line AB.

Zone wise full range stress-strain curves obtained using DIC technique is shown in Fig. 3.12. It can be interpreted from the figure that the FZ (Zone index 4) has a higher yield strength. Strain hardening effect is also predominant in FZ and HAZs which results in lower strain levels in those zones compared to BM. Zone corresponding to BM has lesser yield stress and it is more strained during the tensile testing.

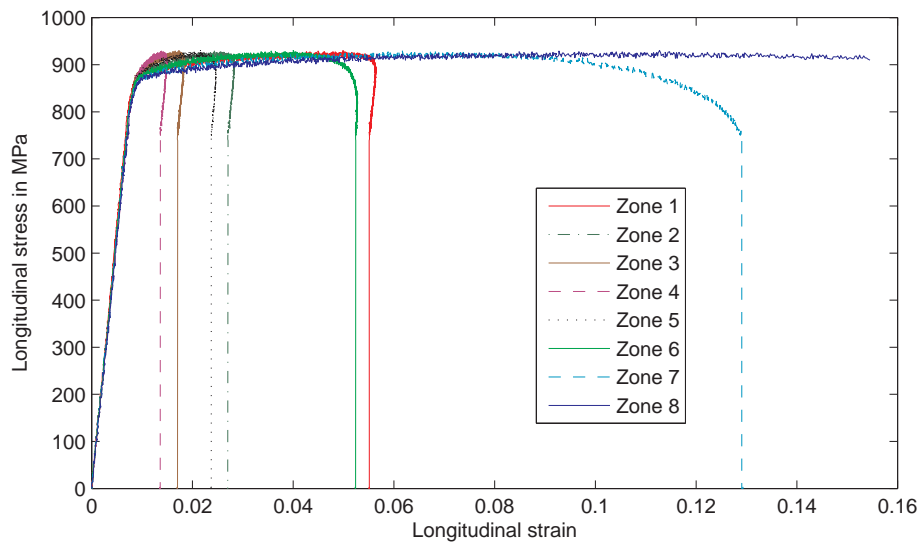


Figure 3.12: Zone wise full range stress-strain curves obtained using DIC technique.

Constitutive parameters corresponding to each zone are extracted from these full range stress-strain curves by using the methodology explained in section 3.4. Material models are fitted into the curves by using least square method. Fig. 3.13 shows the linear and non linear curves fitted on experimental data for parameter extraction and this curve corresponds to zone 6. Similarly curves corresponding to other zones are also used to fit the material models to get the zone wise parameters.

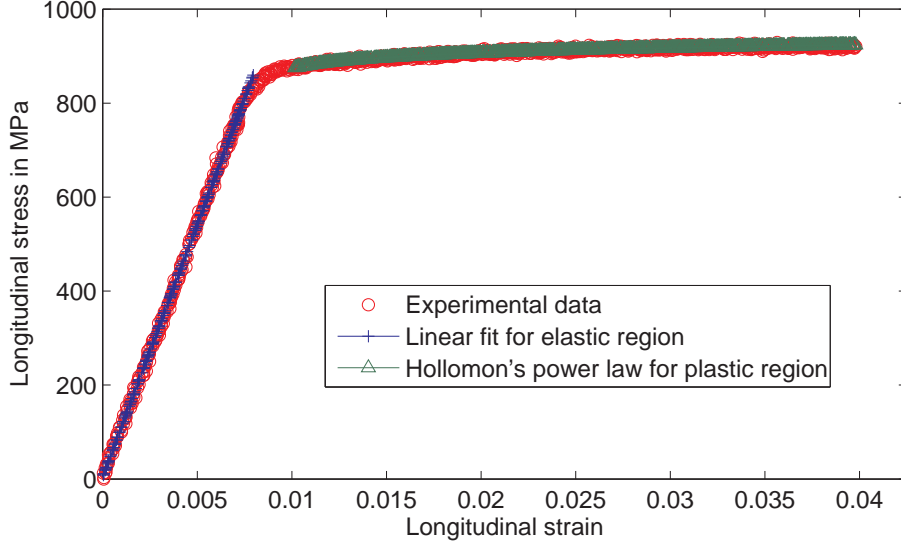


Figure 3.13: Linear and non linear curves fitted on experimental data for parameter extraction corresponding to zone 6.

Young's modulus values obtained for various zones are plotted in Fig. 3.14. It is clear from the figure that the Young's modulus of FZ is less in comparison with other zones and the value increases as one move away from it. BM has reported a Young's modulus value of 110.15 GPa which is the maximum and FZ has reported 101 GPa which correspond to the minimum value of Young's modulus obtained in this study. This difference is in line with the observation reported in [33]. Yilbas *et al.* [47] attributed this variation to the size and cooling rate of the fusion zone and HAZs. Because of the low cooling rates in EBW the ductility of the fusion zone increases and results in a slightly lesser Young's modulus but upon plastic deformation the strain hardening effect dominates and results in considerable reduction in ductility.

Zone wise Poisson's ration variation is depicted in Fig.3.15. The variation is in line with the observation reported in [33]. Poisson's ratio is found to be increasing as one move toward the FZ. In this study FZ has reported a Poisson's ratio of 0.35 and it is the maximum among various other zones. Zone 2 has reported Poisson's ratio value of 0.297 which is the least value among the zone wise Poisson's ratios reported in this study.

Zone wise variation in yield stress is shown in Fig. 3.16. It is clear from the figure that the zone 4 which is FZ has highest yield stress and it decreases towards BM. The least

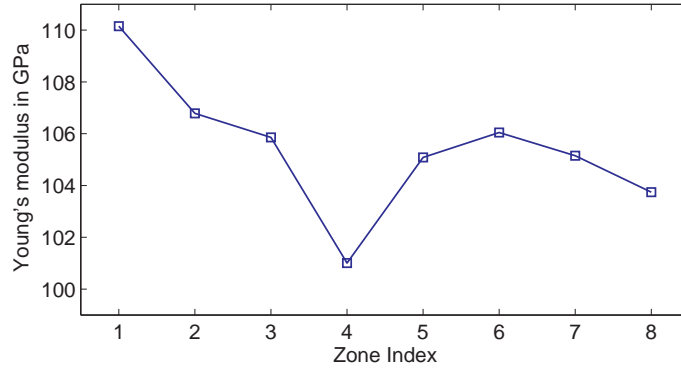


Figure 3.14: Zone wise variation in Young's modulus.

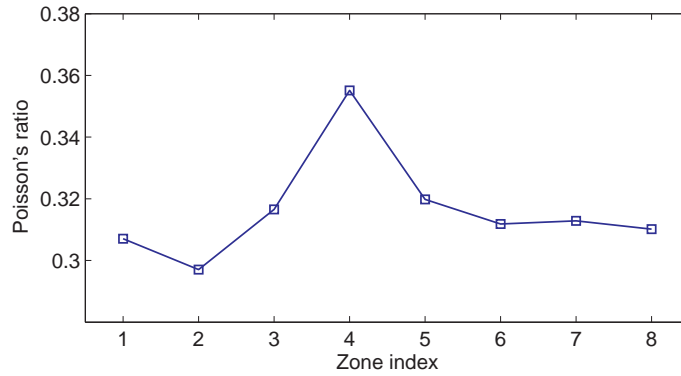


Figure 3.15: Zone wise variation in Poisson's ratio.

value of yield stress is reported for zone 7 which is a base metal zone where final fracture occurred. This variation is in good agreement with the microhardness measurement and location of final fracture. The maximum yield stress value which corresponds to FZ is 907.3 MPa and least value which pertain to failure zone is 870.8 MPa.

Strength coefficient ( $K$ ) variation for the plastic zone is shown in Fig. 3.17. The variation pattern is similar to that of yield stress variation. FZ has the highest  $K$  value and it decreases towards BM. It is a clear indication of predominant hardening of FZ and HAZ's when they deform plastically. Zone 4 which is the FZ has the highest  $K$  value of 1027.6 MPa and zone 8 which is a base metal zone nearer to that of failure zone has the lowest  $K$  value of 958.7 MPa.

Variations in strain hardening exponent ( $n$ ) is depicted in Fig. 3.18. One can clearly interpret from the figure that the HAZs (Zone 3,5) have higher  $n$  value comparing to other zones. FZ also has an  $n$  value higher than that of BM but it is lesser than that of HAZ. Highest recorded  $n$  value is 0.0216 which corresponds to zone 3 and the lowest value is 0.016 which pertain to zone 8. All the zone wise parameters extracted are tabulated in Appendix A.

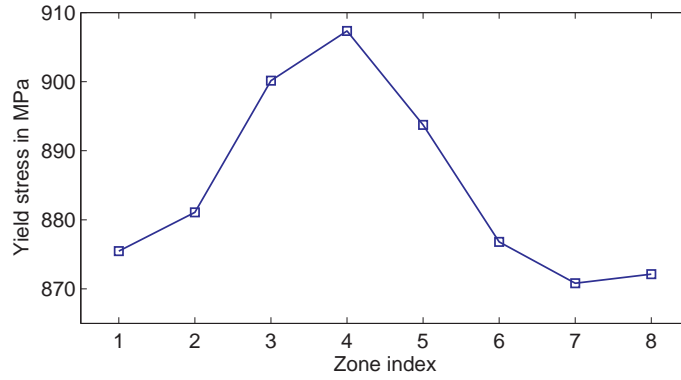


Figure 3.16: Zone wise variation in yield stress.

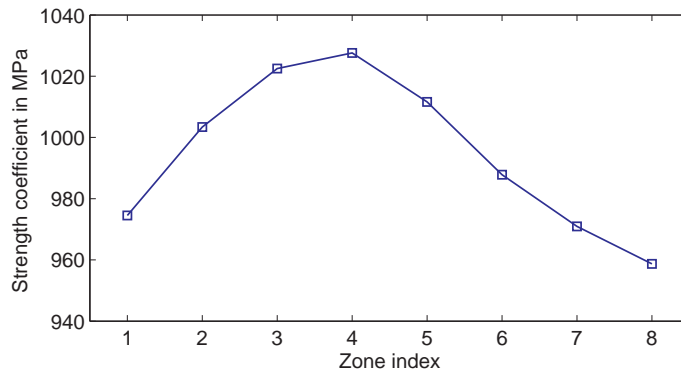


Figure 3.17: Zone wise variation in strength coefficient.

### 3.6 Closure

Zone wise local characterization of electron beam welded (EBW) Ti-6Al-4V alloy has been successfully carried out using digital image correlation technique. Micrographs of various weld zones are utilized for visualizing the changes in microstructure across the weld and also for dividing the area of interest into various zones. As per the micrographic examination it is shown that the fusion zone (FZ) is comprised mostly of  $\alpha$  platelets. Zone wise full range stress-strain curves are extracted for parameter extraction. Following are the main conclusions from the zone wise parameters extracted in this work.

- There is decreasing trend in Young's modulus from base metal (BM) toward the FZ.
- Poisson's ratio of FZ is higher than BM and Heat affected zones (HAZs).
- Yield stress and of FZ is the highest and it reduces as one move towards BM.
- Strength coefficient as given by Hollomon's power law is found to be increasing from BM to FZ.
- HAZs have reported higher strain hardening exponent in comparison with other zones.



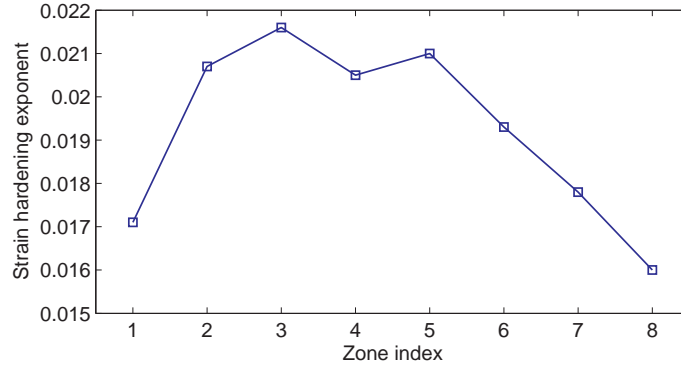


Figure 3.18: Zone wise variation in strain hardening exponent.

Microhardness measurement across the weld indicated the zone wise variation of properties and the extracted constitutive parameters also followed the same trend thereby reassuring the accuracy of the proposed method. Another important information obtained from this zone wise characterization is the yield stress of weakest zone. The failure of all the specimen occurred at the base metal and from the zone wise yield stress extracted it is found that the yield stress of the failure zone is the lowest among various zones. From the above observation it can be concluded that the EBW used to join the Ti-6Al-4V alloy sheets offers superior yield stress and joint strength than that of BM. The obtained zone wise full range stress-strain curves can be utilized as an important input for accurate modelling of the weld for checking the design integrity. The major advantage of local characterization using DIC is the extraction of zone wise full range stress-strain curves from a single tensile testing which is much easier and faster than conventional micro tensile sample testing. The proposed methodology using DIC is found to be effective and accurate in predicting the local constitutive properties over the weld zone and it is highly recommended to implement for various other welding techniques and welding conditions.

## Chapter 4

# Local characterization of welds using virtual fields method involving DIC

### 4.1 Introduction

Virtual fields method is a powerful technique proposed by Grédiac and Pierron [34] which utilizes the surface strain measurements from DIC for solving inverse problems in experimental mechanics. VFM, is based on principle of virtual work (PVW) where the actual whole field strains and kinematically admissible virtual displacement fields are employed for identification of unknown parameters. In this method PVW is employed for writing weak form of local equilibrium equations and solutions of these equations directly results in the extraction of unknown material parameters. In elasticity problems, selection of number of independent and kinematically admissible virtual displacement fields equal to the number of unknown parameters gives a linear system of equations and the sought parameters are extracted by solving this system of equations. In plasticity problems, a cost function is developed by using PVW and appropriate hardening law and plastic parameters are extracted by the minimization of the cost function. The main attractions of VFM are the simplicity, computational speed, lesser data storage requirement, less stringent assumptions, no restrictions on the geometry of the specimen, accuracy and extraction of more number of parameters from lesser number of tests. Pioneered works in the implementation of VFM has come from the research group of Grédiac and Pierron and they have utilized this technique to solve problems pertaining to different fields of experimental mechanics.

In this chapter, VFM is utilized for extracting the zone wise elastic and plastic properties of the same EBW specimen examined in chapter 3. Basic principles, equations and derivations for implementing VFM are discussed. Since the surface strain distribution obtained for the parameter extraction in chapter 3 is used here, the experimental setup, DIC

technique, Material are the same as given in chapter 3. All the parameters extracted using VFM are compared with that of obtained using uniform stress method (USM). Also note that USM is nothing but the method used in chapter 3. Wherever the term ‘USM’ is used in this chapter refers to the study conducted in chapter 3 and basically this chapter is a comparison between the result obtained in chapter 3 with VFM technique.

## 4.2 Material Model

Young’s modulus ( $E$ ) and Poisson’s ratio ( $\nu$ ) are the unknown elastic parameters under investigation. Hollomon’s power law is used as the hardening model for extracting the plastic parameters such as strength coefficient ( $K$ ) and strain hardening exponent ( $n$ ). The constitutive relation for the elastic and plastic parameters are given in Eq. 4.1. where  $\varepsilon_{yy}$  is the total longitudinal strain,  $\sigma_{yy}$  is the corresponding longitudinal stress,  $\sigma_{pl}$  is the stress at proportionality limit,  $\varepsilon_p$  is the longitudinal plastic strain,  $\sigma_{ys}$  is the yield stress which is 0.2% proof stress,  $K$  is the strength coefficient and  $n$  is the strain hardening exponent.

$$\sigma_{yy} = \begin{cases} E\varepsilon_{yy}, & \forall \sigma_{yy} < \sigma_{pl} \\ K\varepsilon_p^n, & \forall \sigma_{yy} > \sigma_{ys} \end{cases} \quad (4.1)$$

In the non linear plastic deformation zone ( $\sigma_{yy} > \sigma_{ys}$ ) the measured strain value is the sum of elastic and plastic strain. So in order to substitute the plastic strain in Eq. (4.1) the approximation given in Eq. 4.2 is used to decouple the plastic strain from the total strain.

$$\varepsilon_p \approx \varepsilon_{yy} - \left( \frac{\sigma_{yy}}{E} \right) \quad (4.2)$$

The constitutive law used in this study for the plastic region is given in Eq. 4.3 which is obtained by substituting Eq. 4.2 in Eq. 4.1.

$$\sigma_{yy} = K \left( \varepsilon_{yy} - \left( \frac{\sigma_{yy}}{E} \right) \right)^n, \forall \sigma_{yy} > \sigma_{ys} \quad (4.3)$$

## 4.3 Weld Zone Identification

Same strain data and weld zones used in chapter 3 is used here. Since the knowledge of zones are important in the virtual field formulation a brief discussion is given here on the zone identification. The Information from micrographic examination and the strain patterns obtained from DIC is utilized here for dividing the area of interest in to various zones. Fig. 4.1(a) shows the surface strain distribution during various load levels during tensile testing. The variation in the longitudinal strain values across the weld can be identified clearly from the figure. FZ and surrounding HAZs are at a lower strain level compared to the

BM indicating a predominant strain hardening on those zones. The region below the weld experiences a higher strain accumulation and necking occurs at that region which leads to the final failure of the specimen. Based on this surface strain distribution pattern and the width of various weld zones measured using micrograph, entire AOI is divided into eight zones as shown in Fig. 4.1(b). The length of each zone are given in Table 4.1. In the divided zones, '4' is FZ, '3' and '5' are HAZs, '2' and '6' are transition zone that is the boundary between HAZ and BM, Zone '7' is the failure zone and '1' and '8' belongs to BM. Zone 7 is the location where the specimen necked and fractured which is identified to obtain the properties of failure zone.

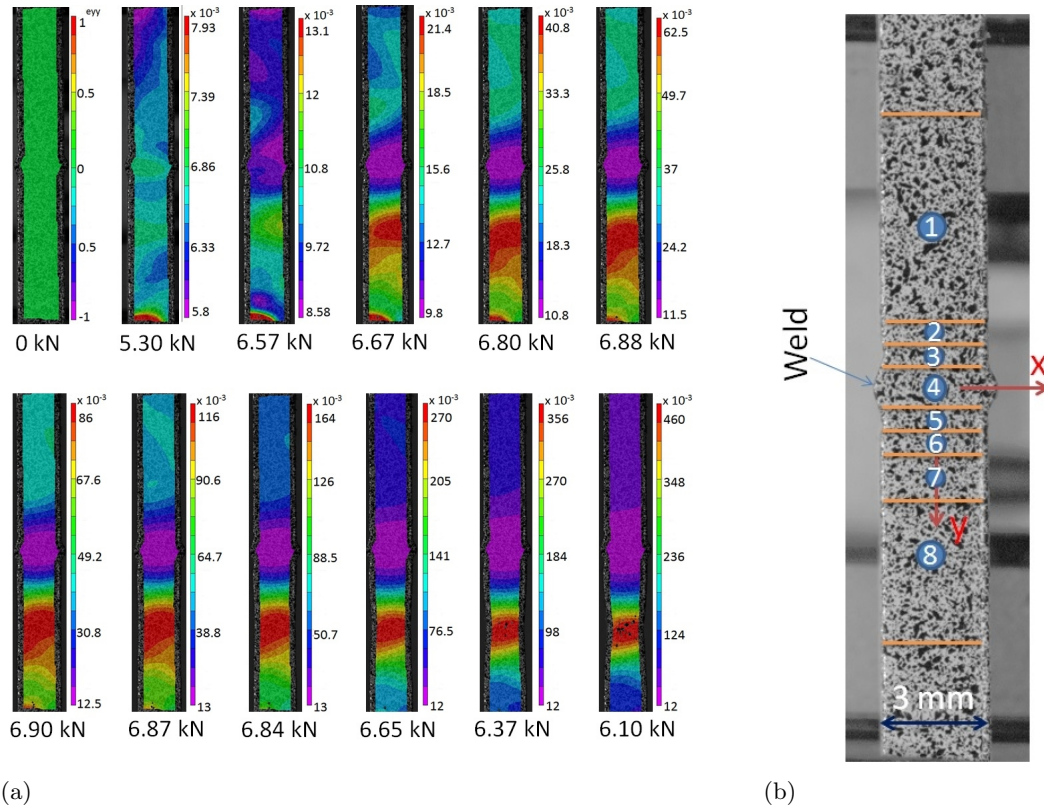


Figure 4.1: Strain evolution and divided AOI (a) Longitudinal strain distribution at various load levels (b) AOI divided into various zones

Table 4.1: Length of various zones which are identified in Fig. 4.1(b)

Zone index	1	2	3	4	5	6	7	8
Length in mm	7	0.8	0.8	1.35	0.8	0.8	2	5

Using image processing tool box of MATLAB<sup>®</sup> the pixels belong to various zones are identified. These zone wise pixels are traced on every load step and strain values corresponding to each zones are identified and stored separately. This information is utilized for plotting full range stress-strain curves of each zone by using USM. In USM it is assumed

that the stress values are constant in all cross-section and it is equal to the ratio of reaction load to the area of cross-section and unknown parameters are identified by fitting the material models on the full range stress-strain curves bu using least square methodology. Material model used in this study is given in section 4.2.

#### 4.4 Virtual Fields Formulation

In this section the basic equations and methodology used for solving elastic and plastic parameters using VFM are discussed in detail. Fig. 4.2 is the free body diagram of the tensile testing showing the displacement and force boundary conditions. Area of interest in the figure is the area over which the strain values are known. ‘Zone x’ is any one of the identified weld zone. The known parameters from the tensile test are the reaction force  $F$ , Surface strain distribution over AOI and the displacement prescribed over  $S_u$ .

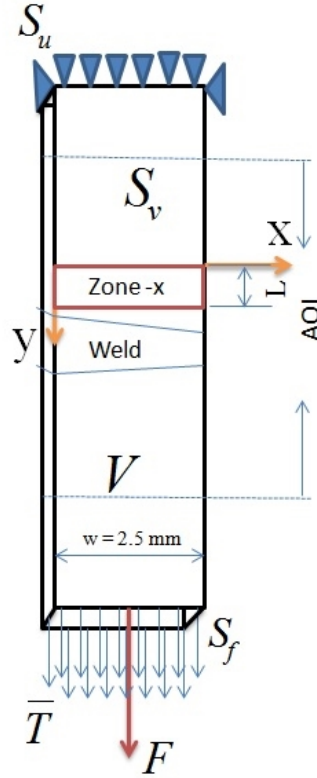


Figure 4.2: Diagram showing the loading and boundary conditions of the tensile testing. ‘AOI’ is the section of specimen where the strains are measured.

Basic governing equation of VFM is given in Equation 4.4. This equation is nothing but the weak form of equilibrium equation derived using the principle of virtual work.

$$-\int_V \sigma_{ij} : \varepsilon_{ij}^* dv + \int_{S_f} \bar{T}_i \cdot u_i^* ds + \int_V b_i \cdot u_i^* dv = \int_V \rho a_i \cdot u_i^* dv \quad (4.4)$$

where:

$V$  is the volume of the element.

$S_v$  is the area ( $x$ - $y$  plane) where the surface strain data is measured using DIC.

$S_f$  is the area where traction boundary condition is applied.

$\sigma_{ij}$  is the stress tensor.

$u_i^*$  is the virtual displacement field which is kinematically admissible.

$\varepsilon_{ij}^*$  is the virtual strain tensor derived from virtual displacement field.

$b_i$  is the volume force vector.

$a_i$  is the acceleration vector.

$\rho$  is the density of the material.

Since the volume forces and inertia forces have negligible contribution towards total work done, Eq. 4.4 can be simplified as given below.

$$\int_V \sigma_{ij} : \varepsilon_{ij}^* dv = \int_{S_f} \bar{T}_i \cdot u_i^* ds \quad (4.5)$$

In a plane stress condition where a two dimensional stress state is existing with the assumption that there is no variation in the stress state along the thickness direction, one can rewire Eq. 4.5 as given in Eq. 4.6. Here  $b$  is the thickness of the specimen.

$$b \int_{S_v} \sigma_{ij} : \varepsilon_{ij}^* ds_v = b \int_w \bar{T}_i \cdot u_i^* dw \quad (4.6)$$

Also, We have reaction force  $F$  corresponding to load step  $t_i$  in terms of traction as given below.

$$b \int_w \bar{T}_i dw = F(t_i) \quad (4.7)$$

On substitution of Eq. 4.7 in Eq. 4.6 we will get

$$\int_{S_v} \sigma_{ij} : \varepsilon_{ij}^* ds_v = \frac{1}{b} F(t_i) \cdot u_i \quad (4.8)$$

Above equation is the simplified form of VFM which is used in this study for elastic and plastic parameter identification and the methodology is explained in the coming subsections.

#### 4.4.1 Elastic Parameter Identification

We have two elastic constants namely Young's modulus and Poisson's ratio to be extracted utilizing the Eq. 4.8. The known quantities from the tensile testing are the strain over the

surface  $S_v$  and Reaction load  $F(t_i)$ . In order to introduce the unknown parameters and actual strain measured using DIC technique into Eq. 4.8, the stress tensor is replaced with the constitutive relation given below. Note that a plane stress assumption is employed and the strain  $\varepsilon_{ij}$  are the actual strains measured over the surface  $S_v$  using DIC technique.

$$\begin{bmatrix} \sigma_{xx} \\ \sigma_{yy} \\ \sigma_{xy} \end{bmatrix} = \begin{bmatrix} \frac{E}{1-\nu^2} & \frac{\nu E}{1-\nu^2} & 0 \\ \frac{\nu E}{1-\nu^2} & \frac{E}{1-\nu^2} & 0 \\ 0 & 0 & \frac{E}{1+\nu} \end{bmatrix} \begin{bmatrix} \varepsilon_{xx} \\ \varepsilon_{yy} \\ \varepsilon_{xy} \end{bmatrix} \quad (4.9)$$

Now Eq. 4.8 can be expanded to the form given in Eq. 4.10 and note that this equation is now have the unknown variables, actual strains measured over the surface  $S_v$ , reaction force  $F(t_i)$ , virtual strains and virtual displacements. It is clear that this equation should satisfy for any kinematically admissible selection of virtual displacement fields. Kinematically admissible means the field which is continuous and satisfies displacement boundary conditions.

$$\begin{aligned} & \frac{E}{1-\nu^2} \left( \int_{S_v} \varepsilon_{xx} \varepsilon_{xx}^* ds_v + \int_{S_v} \varepsilon_{yy} \varepsilon_{yy}^* ds_v \right) + \\ & \frac{\nu E}{1-\nu^2} \left( \int_{S_v} \varepsilon_{xx} \varepsilon_{yy}^* ds_v + \int_{S_v} \varepsilon_{yy} \varepsilon_{xx}^* ds_v \right) + \frac{E}{1+\nu} \left( \int_{S_v} \varepsilon_{xy} \varepsilon_{xy}^* ds_v \right) = \frac{1}{b} F(t_i) u_i^* \end{aligned} \quad (4.10)$$

Since the strain distribution from DIC technique is not a continuous function over the surface but values at discrete points called pixel subset centre above equation can be rewrite as summation over the surface as given below. Here  $N$  is the number of data points on the area of the zone under consideration.

$$\begin{aligned} & \frac{E}{1-\nu^2} \left( \frac{1}{N} \sum_{i=1}^N \varepsilon_{xx} \varepsilon_{xx}^* \Delta s_v + \frac{1}{N} \sum_{i=1}^N \varepsilon_{yy} \varepsilon_{yy}^* \Delta s_v \right) + \\ & \frac{\nu E}{1-\nu^2} \left( \frac{1}{N} \sum_{i=1}^N \varepsilon_{xx} \varepsilon_{yy}^* \Delta s_v + \frac{1}{N} \sum_{i=1}^N \varepsilon_{yy} \varepsilon_{xx}^* \Delta s_v \right) + \\ & \frac{E}{1+\nu} \left( \frac{1}{N} \sum_{i=1}^N \varepsilon_{xy} \varepsilon_{xy}^* \Delta s_v \right) = \frac{1}{b} F(t_i) u_i^* \end{aligned} \quad (4.11)$$

Selection of two independent virtual displacement field will result in two linear independent equations and the unknown parameters ( $E$  and  $\nu$ ) can be extracted by solving this system of equations. Following are the two virtual fields used in this study. Each virtual field are selected in such a way that the material apart from the zone under consideration behaves like a rigid body so that they have no contribution towards internal virtual work. Please refer Fig. 4.2 for the schematic diagram showing a zone and dimension  $L$ .

Virtual field - 1

$$\begin{aligned}
u_{x1}^* &= 0 \text{ and } u_{y1}^* = 0; \text{ for } y < 0 \\
u_{x1}^* &= 0 \text{ and } u_{y1}^* = y; \text{ for } 0 < y < L \\
u_{x1}^* &= 0 \text{ and } u_{y1}^* = L; \text{ for } y \geq L
\end{aligned} \tag{4.12}$$

Corresponding virtual strain fields are:

$$\begin{aligned}
\varepsilon_{xx}^* &= 0, \varepsilon_{yy}^* = 0 \text{ and } \varepsilon_{xy}^* = 0; \text{ for } y < 0 \\
\varepsilon_{xx}^* &= 0, \varepsilon_{yy}^* = 1 \text{ and } \varepsilon_{xy}^* = 0; \text{ for } 0 < y < L \\
\varepsilon_{xx}^* &= 0, \varepsilon_{yy}^* = 0 \text{ and } \varepsilon_{xy}^* = 0; \text{ for } y \geq L
\end{aligned} \tag{4.13}$$

Virtual field - 2

$$\begin{aligned}
u_{x2}^* &= 0 \text{ and } u_{y2}^* = 0; \text{ for } y < 0 \\
u_{x2}^* &= \left(x - \frac{w}{2}\right) y (y - L) \text{ and } u_{y2}^* = y; \text{ for } 0 < y < L \\
u_{x2}^* &= 0 \text{ and } u_{y2}^* = 0; \text{ for } y \geq L
\end{aligned} \tag{4.14}$$

Corresponding virtual strain fields are:

$$\begin{aligned}
\varepsilon_{xx}^* &= 0, \varepsilon_{yy}^* = 0 \text{ and } \varepsilon_{xy}^* = 0; \text{ for } y < 0 \\
\varepsilon_{xx}^* &= y(y - L), \varepsilon_{yy}^* = 0 \text{ and } \varepsilon_{xy}^* = \frac{1}{2} \left(2xy - xL - wy + \frac{w}{2}L\right); \text{ for } 0 < y < L \\
\varepsilon_{xx}^* &= 0, \varepsilon_{yy}^* = 0 \text{ and } \varepsilon_{xy}^* = 0; \text{ for } y \geq L
\end{aligned} \tag{4.15}$$

Substituting virtual field-1 and virtual field-2 in Eq. 4.11 we will get two equations as shown below. Also note that here  $\Delta S_v$  is the area of the zone under consideration.

$$\frac{E}{1 - \nu^2} \left( \frac{1}{N} \sum_{i=1}^N \varepsilon_{yy} \right) \Delta S_v + \frac{\nu E}{1 - \nu^2} \left( \frac{1}{N} \sum_{i=1}^N \varepsilon_{xx} \right) \Delta S_v = \frac{1}{b} F(t_i) L \tag{4.16}$$

$$\begin{aligned}
&\frac{E}{1 - \nu^2} \left( \frac{1}{N} \sum_{i=1}^N \varepsilon_{xx} y (y - L) \right) \Delta S_v + \frac{\nu E}{1 - \nu^2} \left( \frac{1}{N} \sum_{i=1}^N \varepsilon_{yy} (y - L) y \right) \Delta S_v + \\
&\frac{E}{1 + \nu} \left( \frac{1}{N} \sum_{i=1}^N \varepsilon_{xy} \frac{1}{2} \left( 2xy - xL - wy + \frac{w}{2}L \right) \right) \Delta S_v = 0
\end{aligned} \tag{4.17}$$

For all the eight zones identified the above set of equations are solved by inputting known zone wise surface strain values from DIC technique and reaction load value from the load cell reading. Area of the fusion zone, where a weld reinforcement is present, is measured



by counting the number of pixels belonging to that zone from a calibrated image using MATLAB<sup>®</sup> image processing toolbox.

#### 4.4.2 Plastic Parameter Identification

Since the strain evolution upon loading is non-linear in the plastic deformation region it is not possible to extract the required parameters from a single strain distribution and load data as in case of elasticity. But at various load levels this non-linearity will give rise to independent system of equations even against a single chosen virtual displacement field. This property is used by Grédiac *et al.* [40] for formulating a minimization problem to extract the plastic constitutive parameters. Here, in order to solve for the unknown material parameters, the virtual displacement field given in Eq. 4.12 is used. Upon substitution of this virtual displacement and corresponding virtual strains in Eq. 4.8 we will get Eq. 4.18.

$$\int_{S_v} \sigma_{ij} ds_v = \frac{1}{b} F(t_i) L \quad (4.18)$$

Now by replacing  $\sigma_{ij}$  with the material model given in Eq. 3.3.2 one can write Eq 4.18 as given below.

$$\int_{S_v} K \left( \varepsilon_{yy} - \left( \frac{\sigma_{ys}}{E} \right) \right)^n ds_v = \frac{1}{b} F(t_i) L \quad (4.19)$$

Eq. 4.20 is obtained by changing the integration operation in Eq. 4.19 to summation over the area and  $N$  is the number of measurement points in the zone under consideration.

$$\frac{1}{N} \sum_{i=1}^N K \left( \varepsilon_{yy} - \left( \frac{\sigma_{ys}}{E} \right) \right)^n \Delta s_v = \frac{1}{b} F(t_i) L \quad (4.20)$$

The known parameters in the above equation are  $E$  obtained from the elastic analysis,  $N$ ,  $\varepsilon_{yy}$ ,  $\Delta s_v$ ,  $F(t_i)$ ,  $L$  and  $b$ . In order to solve for the unknown values ( $K$ ,  $n$  and  $\sigma_{ys}$ ) a cost function is developed as shown below.

$$f = \sum_{t_1}^{t_n} \left[ \frac{1}{N} \sum_{i=1}^N K \left( \varepsilon_{yy} - \left( \frac{\sigma_{ys}}{E} \right) \right)^n \Delta s_v - \frac{1}{b} F(t_i) L \right]^2 \quad (4.21)$$

$t_1, t_2 \dots t_n$  are the load steps selected in the plastic deformation region. Minimization of the cost function given in Eq. 4.21 results in the direct identification of the unknown parameters.

In this study a derivative free multi variable optimization scheme, Nelder-Mead algorithm [60] is used for solving for the unknowns. Nelder-Mead algorithm also known as downhill simplex method is a technique for minimizing an objective function in a many-dimensional space. It requires an initial guess to start with. Even though any reasonable initial guess will result in consistent results, in this study the parameters close to virgin

material properties are chosen as the initial guess since it can result in faster convergence. Optimization toolbox of MATLAB<sup>®</sup> is utilized for the minimization. 27 load steps in the plastic deformation region is used for FZ and HAZ zones. For BM region, 45 load steps are used because BM have a larger plastic deformation region compared to FZ and HAZs. A fast convergence rate is observed for the parameter extraction. In less than two minutes parameters pertaining to each zone are obtained by running the optimization scheme in a PC with Intel<sup>®</sup> core<sup>™</sup> i3-2370M processor @ 2.40 GHz with a RAM of 4 GB.

Form both elastic and plastic parameter estimation methodologies explained above, one can observe that the VFM formulation is independent of the geometry of the test specimen. If the whole field surface strain distribution is available over the specimen having any geometry, then proper selection of kinematically admissible virtual fields can extract the unknown parameters without using assumptions such as uniform stress distribution. In the present case, above property of VFM is a clear advantage over USM since the weld reinforcement, which introduces a change in cross-section at the middle of the tensile samples is not removed from the tensile samples.

## 4.5 Results and Discussions

This section discuss in detail the parameters extracted from the tensile testing and micro-hardness measurements. Also the results obtained using USM and VFM techniques are compared.

### 4.5.1 Observations From Tensile Test

Location of fracture is an important observation for transverse weld tensile testing. Fig. 4.3 shows the specimen fractured during tensile testing. It can be observed from the figure that the fracture occurred away from the FZ, at BM but near to HAZ (Zone 7 given in Fig. 3.7(b)). Since the fracture is not in FZ and HAZs, it can be interpret that the weld has a strength over match in comparison with the BM.

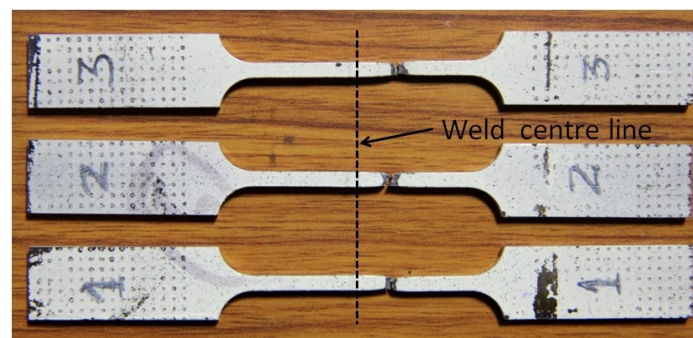


Figure 4.3: Fractured specimens after tensile testing.

Zone wise stress strain curves obtained using USM is shown in Fig. 3.12. It can be

interpreted from the figure that there is a variation in yield stress from zone to zone. The curve corresponds to FZ has yielded at higher level of stress and it experienced least amount of strain before the fracture of specimen. Parameter extraction using USM is done using fitting material model onto the experimental curves as explained in subsection 4.3. Fig. 3.13 shows the experimental stress-strain curve with material models fitted onto it.

#### 4.5.2 Local parameters using USM and VFM

Zone wise Young's modulus obtained using USM and VFM are shown in Fig. 4.4 and the percentage variation of the parameters extracted using VFM from USM are tabulated in Table 4.2. The trend in variation of  $E$  obtained using both the techniques indicates that there is a reduction in  $E$  value as one move from BM towards FZ (zone 4). This variation is in line with the observations reported in [22, 33]. This variation in  $E$  value is not expected and in case of miniature tensile test this variation is not generally observed. But it is a well known fact that the locked in thermal stresses in the form of tensile and compressive residual stress surrounding the weld can affect the performance of the weld. From literatures [48–50, 61] it is clear that the FZ is experiencing high tensile residual stresses which are comparable or greater than the yield stress of the base material and it gradually reducing to distributed compressive stress field towards the BM. Since no post weld heat treatment has been done on the welded specimens used in this study the tensile residual stresses at FZ might have caused the reduction in Young's modulus. Yilbas *et al.* [47] attributed this variation to the size and cooling rate of the fusion zone. It is clear from the Fig. 4.4 and Table 4.2 that the parameters extracted using VFM is in good agreement with those extracted using USM.

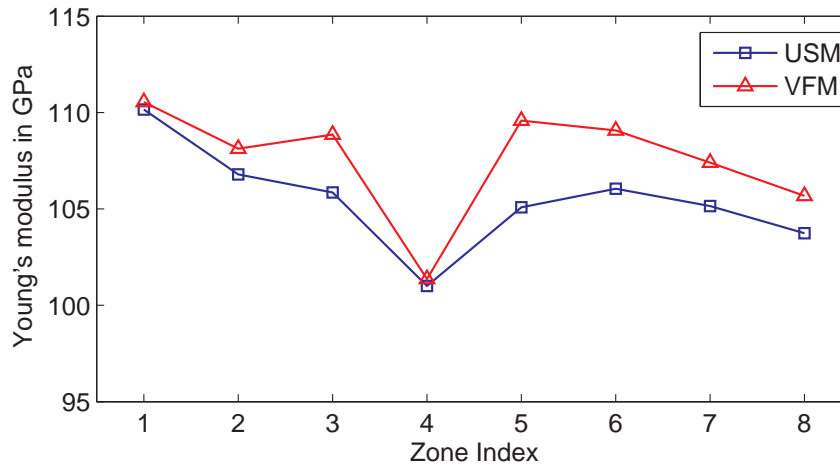


Figure 4.4: Comparison of zone wise variation in Young's modulus obtained using USM and VFM.

Variations in Poisson's ratio across the weld is shown in Fig. 4.5 and Table 4.3 gives the percentage variation of Poisson's ratio extracted using VFM from that of extracted using

Table 4.2: Percentage deviation of zone wise Young’s modulus extracted using VFM from that of extracted using USM

Zone index	1	2	3	4	5	6	7	8
% variation from USM	0.35	1.24	2.76	0.35	4.10	2.77	2.10	1.83

USM. The zone wise trend of Poisson’s ratio is in line with the observation reported by [33]. Here FZ has reported a higher poisson ratio and it decreases as one move away from FZ. Even though the trend of Poisson’s ratio variation is same for both VFM and USM techniques there is a considerable deviation of values estimated using VFM from USM. This variation is primarily due to the noise in the strain distribution obtained from the DIC technique. Pierron *et al.* [37] have conducted a sensitivity study of VFM on the effect of noise in the extracted parameters by adding simulated noise in to the VFM input data. They concluded that the Poisson’s ratio is the quantity greatly affected by noise and all other extracted parameters showed reasonable consistency.

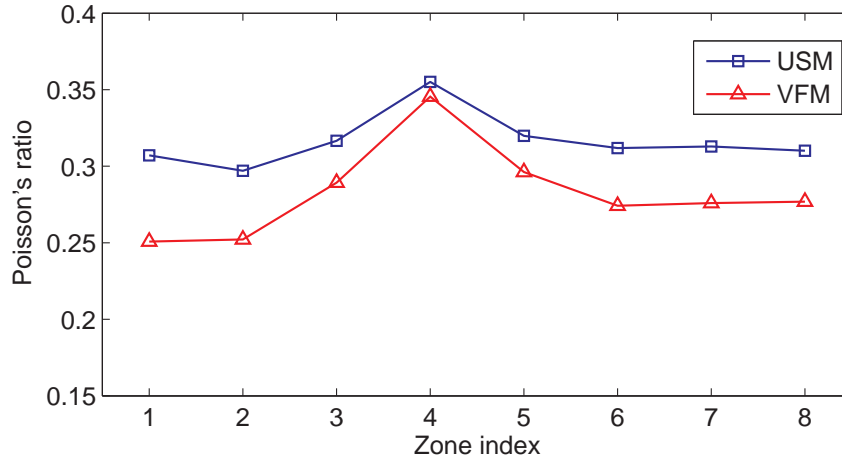


Figure 4.5: Comparison of zone wise variation in Poisson’s ratio obtained using USM and VFM.

Table 4.3: Percentage deviation of zone wise Poisson’s ratio extracted using VFM from that of extracted using USM

Zone index	1	2	3	4	5	6	7	8
% variation from USM	-22.42	-17.80	-9.43	-2.80	-7.97	-13.73	-13.37	-12.03

Fig. 4.6 shows the comparison between zone wise strength coefficient ( $K$ ) extracted using VFM and USM. Percentage variation of the  $K$  value extracted using VFM from that of USM is tabulated in Table 4.4. It is clear from the figure and table that parameters extracted using both the methods are in good agreement. The FZ has shown a higher  $K$  value and it decreased toward BM. Least  $K$  value is reported for ‘zone 8’ followed by ‘zone

7' where the final fracture occurred.

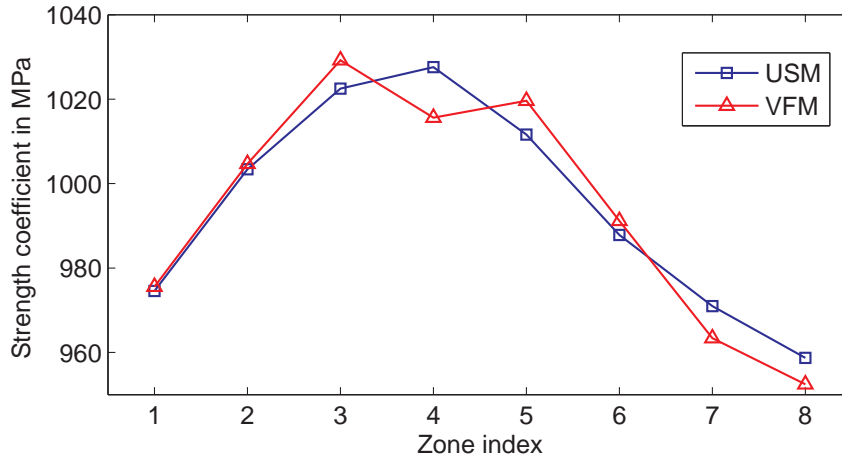


Figure 4.6: Comparison of zone wise variation in strength coefficient obtained using USM and VFM.

Table 4.4: Percentage deviation of zone wise strength coefficient extracted using VFM from that of extracted using USM

Zone index	1	2	3	4	5	6	7	8
% variation from USM	0.10	0.13	0.65	-1.18	0.79	0.34	-0.79	-0.66

Zone wise strain hardening exponent ( $n$ ) extracted using USM and VFM is shown in Fig. 4.7 and the percentage deviation of the values extracted using VFM from that of USM are tabulated in Table 4.5. One can observe from the figure that the values extracted using both the method are in good agreement. The deviation between  $n$  values extracted using VFM and USM is higher for FZ followed by HAZ. This variation can be due to the variation in cross-section of FZ because of the presence of weld reinforcement, which will affect the uniform stress assumption because the actual stress field in FZ is not uniform due to this change in geometry. This can affect the parameters extracted using USM and hence the deviation from VFM is higher in FZ. The FZ has reported a higher hardening exponent and it decreased towards the BM.

Table 4.5: Percentage deviation of zone wise strain hardening exponent extracted using VFM from that of extracted using USM

Zone index	1	2	3	4	5	6	7	8
% variation from USM	2.29	1.74	6.97	14.54	7.95	4.91	4.29	2.69

Fig. 4.8 shows the zone wise yield stress estimated using VFM and USM. Percentage variation of yield stress estimated using VFM from that of estimated using USM is shown in Table 4.6 and it can be observed that the yield stress values extracted using both the

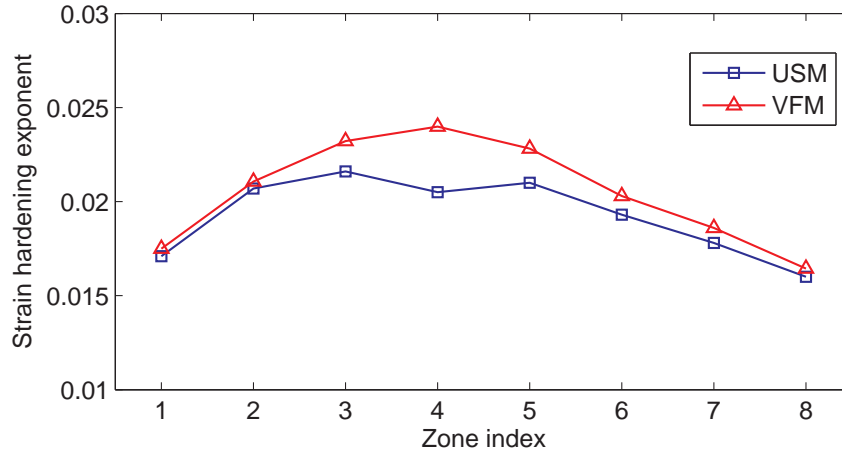


Figure 4.7: Comparison of zone wise variation in strain hardening exponent obtained using USM and VFM.

methods are close to each other. In a similar study conducted by Sutton *et al.* [19] the yield stress values extracted using VFM resulted in a lower estimate of yield stress compared to USM. They pointed out that the lower estimate of yield stress using VFM is due to the simultaneous extraction of all the zone wise properties together by minimization performed using a single cost function over entire zones. In this study the minimization of the cost function is performed zone wise which led lesser number of variables per optimization operation and resulted in better yield stress estimates. It is clear from the figure that FZ have higher yield stress and it decreases as one move towards BM. The lowest yield stress is reported for ‘zone 7’ which is a BM zone where the final fracture is observed. All the zone wise parameters extracted are tabulated in Appendix B.

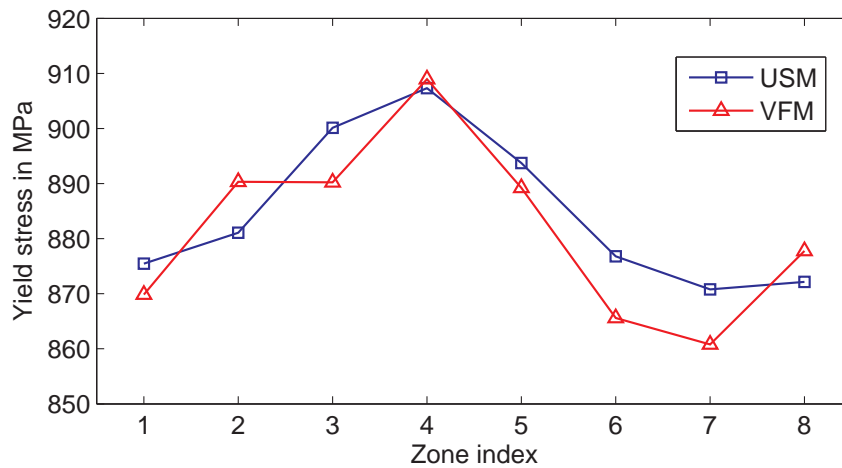


Figure 4.8: Comparison of zone wise variation in yield stress obtained using USM and VFM.

Table 4.6: Percentage deviation of zone wise yield stress extracted using VFM from that of extracted using USM

Zone index	1	2	3	4	5	6	7	8
% variation from USM	-0.65	1.04	-1.11	0.18	-0.51	-1.29	-1.16	0.64

## 4.6 Closure

In the present study, virtual field method (VFM) has been successfully implemented for the characterization of a electron beam weld on Ti-6Al-4V titanium alloy by involving digital image correlation (DIC) technique. Two methodologies namely uniform stress method (USM) and VFM are compared. The comparison of properties extracted using both the methods are in good agreement. Micrographic examination of the weld is performed for identification of various thermally affected zones. Fusion zone (FZ) has a higher Yield strength, hardening exponent and Poisson's ratio but the Young's modulus of FZ is found to be the minimum in comparison with other zones. Specimen fracture during tensile testing is observed at base metal near to heat affected zones and the yield stress obtained for the failure zone is the least in both USM and VFM methodologies. Microhardness variation across the weld has also followed the same trend as that of the zone wise yield stress variation which reassured the effectiveness of the proposed methods. VFM has clear advantages over USM in weld zone characterization because in VFM there is no requirement of stresses to be constant in all the cross-sections and it give one the flexibility to test the weld specimens without removing the weld reinforcement. VFM, as proposed in this study is found to be highly suitable for zone wise characterization of weld because of its less stringent assumptions, ability to extract the properties from zones having variable geometries such as FZ with weld reinforcement, faster convergence, computational simplicity, lesser data storage requirement, accuracy etc. Because of the benefits listed above and from the results obtained from the present study it is highly recommended to use VFM for zone wise characterisation of welds.

## Chapter 5

# Conclusions and Future Recommendations

### 5.1 Conclusions

In this study, the local zone wise characterization of welds have been successfully carried out using the surface strain measurement from digital image correlation technique (DIC). Young's modulus, Poisson's ratio, yield stress, strength coefficient and strain hardening exponent are the parameters extracted for each weld zone. Uniform stress method (USM) involving DIC is implemented for extracting the zone wise elastic and plastic parameters of a bead-on-plate weld produced using twin wire gas metal arc weld on mild steel sheet. The extracted local parameters are compared with the global properties of the weld and with virgin material properties. A new methodology by utilizing the surface strain distribution obtained using DIC and micrographic observation is proposed for accurate identification of various thermally affected zones from a speckled DIC image. Zone wise full range stress-strain curves are plotted using uniform stress assumption. Hollomon's power law is used as the hardening rule for plastic zone characterization. A Vicker's microhardness measurement is also conducted to study the variation of hardness across the weld and to compare the trend of hardness variation with zone wise variation of yield stress obtained using USM involving DIC. Fusion zone of the weld deposition has reported a higher Yield strength and microhardness and both found decreasing towards base metal. Young's modulus is found to be decreasing as one move from basemetal towards fusion zone.

After the successful implementation of USM on the bead-on-plate weld zone characterization, the same methodology is utilized to characterize various zones of a through thickness electron beam weld on Ti-6Al-4V titanium alloy. Here the fusion zone has reported a higher yield strength, microhardness, strength coefficient, strain hardening exponent and Poisson's ratio. Young's modulus of fusion zone is reported to be in a lower side and it is found to be increasing as one move towards the base metal.



Virtual fields method (VFM), which is a more advanced and faster material characterization technique has been implemented for extracting zone wise material properties of a through thickness electron beam weld on Ti-6Al-4V titanium alloy. It is for the first time VFM is successfully used for extracting the zone wise elastic properties of a weld. Results obtained using VFM are compared with that of extracted using USM and it is found that both are in good agreement.

## 5.2 Future Recommendations

There are many fields where the knowledge of zone wise local properties of a weld can be utilized for improvements in design or product performance. First of this kind is a finite element modelling of a weld using the zone wise properties for its entire stress strain range. Proposed methods (USM and VFM) can be implemented for characterizing thin sheet metal welds. Functionally graded material characterization is one of the best suitable field in which the local characterization can play an important role in process and product improvement studies. High temperature behaviour of various welds zones is one of the important research area where local behaviour at various elevated temperatures can be studied using proposed methodologies. Local characterization using DIC can be used for the comparison study between the property distribution across the weld for different welding techniques. Also, sensitivity analysis of VFM for quantifying the effect of image noise and other DIC parameters on the result is a highly recommended study to minimize the error in the results obtained using VFM.

## Publications

- K. M. Saranath, Abhay Sharma, M. Ramji, Zone wise local characterization of welds using digital image correlation technique, Optics and Lasers in Engineering 63 (2014) 30-42.

## Under Submission

- K. M. Saranath, Abhay Sharma, M. Ramji, Investigation of local zone wise elastic and plastic properties of electron beam welded Ti-6Al-4V alloy using digital image correlation
- K. M. Saranath, Abhay Sharma, M. Ramji, Local zone wise elastic and plastic properties of electron beam welded Ti-6Al-4V alloy using digital image correlation: A comparison between uniform stress and virtual fields method

## Conferences

- Saranath K M, Naresh Reddy Kolanu, Ramji M, Material characterization of Al 2014 T6 aluminum alloy using virtual fields method, ISEM 2014, New Delhi - Abstract accepted
- Saranath K M, R Harilal, Mohammad Kashfuddoja and Ramji M, Material characterization of carbon fiber reinforced polymer laminate using virtual fields method , ICTACEM 2014, IIT Kharagpur - Under review

## Appendix A

# Zone Wise Parameters Obtained for Ti-6Al-4V EBW Sample Using USM

Table A.1: Zone wise parameters extracted for Ti-6Al-4V EBW Sample Using USM

Zone index	$E$ in GPa	Poisson's ratio	$\sigma_{ys}$ in MPa	$K$ in MPa	$n$
1	110.15	0.307	875.46	974.53	0.0171
2	106.78	0.297	881.06	1003.4	0.0207
3	105.85	0.316	900.13	1022.5	0.0216
4	101.00	0.355	907.33	1027.6	0.0205
5	105.08	0.319	893.73	1011.6	0.0210
6	106.04	0.312	876.80	987.82	0.0193
7	105.14	0.313	870.80	970.95	0.0178
8	103.74	0.310	872.13	958.71	0.0160

## Appendix B

# Zone Wise Parameters Obtained for Ti-6Al-4V EBW Sample Using VFM

Table B.1: Zone wise parameters extracted for Ti-6Al-4V EBW Sample Using VFM

Zone index	$E$ in GPa	Poisson's ratio	$\sigma_{ys}$ in MPa	$K$ in MPa	$n$
1	110.54	0.251	869.83	975.55	0.0175
2	108.12	0.252	890.32	1004.6	0.0210
3	108.86	0.289	890.21	1029.2	0.0232
4	101.36	0.345	908.96	1015.6	0.0239
5	109.58	0.296	889.23	1019.6	0.0228
6	109.07	0.274	865.61	991.15	0.0202
7	107.40	0.276	860.79	963.37	0.0185
8	105.67	0.277	877.78	952.43	0.0164

# References

- [1] R. W. Messler. Principles of welding: Processes, Physics, Chemistry and metallurgy, 1–16. Wiley-VCH Verlag GmbH, 2004.
- [2] A. I. H. Committee and D. L. Olson, eds. ASM handbook: Welding, brazing, and soldering, volume 6 of *ASM Handbook*. ASM International, 1993.
- [3] K. Weman. Welding processes handbook. CRC Press LLC, Boca Raton, New York, 2011.
- [4] G. Trommer. Tandem wire process improves ship panel production. *Weld. J* 88, (2009) 42–9.
- [5] K.-B. Lee, C. Kim, and D.-S. Kim. High deposition rate pulse gas metal arc welding for Al 5083 thick plate. *Proceedings of the Institution of Mechanical Engineers, Part B: Journal of Engineering Manufacture* 227, (2013) 848–854.
- [6] A. Scotti, C. O. Morais, and L. O. Vilarinho. The effect of out-of-phase pulsing on metal transfer in twin-wire GMA welding at high current level. *Welding journal* 85, (2006) 225–230.
- [7] Y. Hirata. Pulsed arc welding. *Welding international* 17, (2003) 98–115.
- [8] W. H. Peters and W. F. Ranson. Digital imaging techniques in experimental stress analysis. *Optical Engineering* 21, (1982) 213,427–213,427.
- [9] M. A. Sutton, W. J. Wolters, W. H. Peters, W. F. Ranson, and S. R. McNeill. Determination of displacements using an improved digital correlation method. *Image and vision computing* 1, (1983) 133–139.
- [10] M. A. Sutton, J. H. Yan, V. Tiwari, H. W. Schreier, and J. J. Orteu. The effect of out-of-plane motion on 2D and 3D digital image correlation measurements. *Optics and Lasers in Engineering* 46, (2008) 746–757.
- [11] T. C. Chu, W. F. Ranson, and M. A. Sutton. Applications of digital-image-correlation techniques to experimental mechanics. *Experimental Mechanics* 25, (1985) 232–244.

- [12] B. Pan, K. Qian, H. Xie, and A. Asundi. Two-dimensional digital image correlation for in-plane displacement and strain measurement: a review. *Measurement science and technology* 20, (2009) 062,001.
- [13] M. A. Sutton, J. J. Orteu, and H. W. Schreier. Image correlation for shape, motion and deformation measurements: basic concepts, theory and applications. Springer, New York, 2009.
- [14] Z. Hu, H. Xie, J. Lu, H. Wang, and J. Zhu. Error evaluation technique for three-dimensional digital image correlation. *Applied Optics* 50, (2011) 6239–6247.
- [15] P. Reu. A study of the influence of calibration uncertainty on the global uncertainty for digital image correlation using a Monte Carlo approach. *Experimental Mechanics* 53, (2013) 1661–1680.
- [16] Correlated Solutions, Inc., 121 Dutchman Blvd, Columbia, SC 29063-USA. Vic-2D Reference Manual 2009.
- [17] H. Schreier and M. Sutton. Systematic errors in digital image correlation due to undermatched subset shape functions. *Experimental Mechanics* 42, (2002) 303–310.
- [18] B. Pan. Bias error reduction of digital image correlation using Gaussian pre-filtering. *Optics and Lasers in Engineering* 51, (2013) 1161 – 1167.
- [19] M. A. Sutton, J. H. Yan, S. Avril, F. Pierron, and S. M. Adeb. Identification of Heterogeneous Constitutive Parameters in a Welded Specimen: Uniform Stress and Virtual Fields Methods for Material Property Estimation. *Experimental Mechanics* 48, (2008) 451–464.
- [20] D. Gautam, D. Mousumi, S. Subhasis, K. G. Kalyan, C. Sanchita, and K. R. Ashok. Characterization of cast stainless steel weld pools by using ball indentation technique. *Materials Science and Engineering: A* 513-514, (2009) 389 – 393.
- [21] G. Liu, L. E. Murr, C. S. Niou, J. C. McClure, and F. R. Vega. Microstructural aspects of the friction-stir welding of 6061-T6 aluminum. *Scripta Materialia* 37, (1997) 355 – 361.
- [22] R. R. Ambriz, D. Chicot, N. Benseddiq, G. Mesmacque, and S. D. de la Torre. Local mechanical properties of the 6061-T6 aluminium weld using micro-traction and instrumented indentation. *European Journal of Mechanics - A/Solids* 30, (2011) 307 – 315.
- [23] D. A. LaVan. Microtensile properties of weld metal. *Experimental Techniques* 23, (1999) 31–34.

- [24] S. M. Zuniga and S. D. Sheppard. Determining the constitutive properties of the heat-affected zone in a resistance spot weld. *Modelling and Simulation in Materials Science and Engineering* 3, (1995) 391–416.
- [25] R. K. Naresh and M. Ramji. Material characterisation of Al-2024 T6 alloy using 3D-digital image correlation technique. In Proceedings of International conference on metallurgical and materials Processes, products and applications. OPJIT International Journal of Innovation and Research, Raigarh, India, 2014 .
- [26] W. D. Lockwood and A. P. Reynolds. Simulation of the global response of a friction stir weld using local constitutive behavior. *Materials Science and Engineering: A* 339, (2003) 35–42.
- [27] C. Leitão, I. Galvão, R. Leal, and D. Rodrigues. Determination of local constitutive properties of aluminium friction stir welds using digital image correlation. *Materials and Design* 33, (2012) 69 – 74.
- [28] F. T. Duvall. Full field strain measurement in welds. Master’s thesis, College of Engineering, University of South Carolina 1998.
- [29] A. P. Reynolds and F. Duvall. Digital Image Correlation for Determination of Weld and Base Metal Constitutive Behavior. *Welding research supplement* 355–360.
- [30] M. Acar, S. Gungor, S. Ganguly, P. J. Bouchard, and M. E. Fitzpatrick. Variation of Mechanical Properties in a Multi-pass Weld Measured Using Digital Image Correlation. In Proceedings of the SEM annual conference. Albuquerque, New Mexico, 2009 .
- [31] M. De Strycker, P. Lava, W. Van Paepegem, L. Schueremans, and D. Debruyne. Measuring welding deformations with the digital image correlation technique. *Welding Journal* 90, (2011) 107–112.
- [32] J. Yan, M. A. Sutton, A. P. Reynolds, A. Samer, and D. Horsley. Characterization of heterogeneous response of pipeline steel weld using digital image correlation. In Proceedings of the 2006 SEM annual conference and exposition on experimental and applied mechanics. St Louis, Missouri, USA, 2006 90–96.
- [33] G. R. Song, C. F. He, X. Y. Li, Z. H. Liu, and B. Wu. Determining the Change of the HAZ Mechanical Properties of TA15 Titanium Alloy by Electron Beam Welding with Ultrasonic Method. In Proceedings of the Second International Conference on Heterogeneous Materials Mechanics. Huangshan, China, 2008 1362 – 1365.
- [34] F. Pierron and M. Grédiac. The virtual fields method: extracting constitutive mechanical parameters from full-field deformation measurements. Springer, New York, 2012.

- [35] M. Grédiac, F. Pierron, S. Avril, and E. Toussaint. The Virtual Fields Method for Extracting Constitutive Parameters From Full-Field Measurements: a Review. *Strain* 42, (2006) 233–253.
- [36] S. Avril, M. Bonnet, A.-S. Bretelle, M. Grédiac, F. Hild, P. Ienny, F. Latourte, D. Lemosse, S. Pagano, E. Pagnacco et al. Overview of identification methods of mechanical parameters based on full-field measurements. *Experimental Mechanics* 48, (2008) 381–402.
- [37] F. Pierron and M. Grédiac. Identification of the through-thickness moduli of thick composites from whole-field measurements using the Iosipescu fixture: theory and simulations. *Composites Part A: Applied Science and Manufacturing* 31, (2000) 309–318.
- [38] M. Grédiac, E. Toussaint, and F. Pierron. Special virtual fields for the direct determination of material parameters with the virtual fields method. 1—Principle and definition. *International Journal of Solids and Structures* 39, (2002) 2691–2705.
- [39] E. Toussaint, M. Grédiac, and F. Pierron. The virtual fields method with piecewise virtual fields. *International Journal of Mechanical Sciences* 48, (2006) 256–264.
- [40] M. Grédiac and F. Pierron. Applying the virtual fields method to the identification of elasto-plastic constitutive parameters. *International Journal of Plasticity* 22, (2006) 602–627.
- [41] G. Le Louëdec, F. Pierron, M. Sutton, and A. Reynolds. Identification of the Local Elasto-Plastic Behavior of FSW Welds Using the Virtual Fields Method. *Experimental Mechanics* 53, (2013) 849–859.
- [42] ASTM Standard E8/E8M-11, Standard Test Methods for Tension Testing of Metallic Materials. ASTM International, 2011.
- [43] J. H. Hollomon. *Trans. AIME* 162, (1945) 268–290.
- [44] ASTM Standard E646-07, Standard Test Method for Tensile Strain-Hardening Exponents (n -Values) of Metallic Sheet Materials. ASTM International, 2007.
- [45] W. F. Hosford. *Mechanical Behavior of Materials*. Cambridge University Press, New York, 2005.
- [46] ASTM Standard E132-04, Standard Test Method for Poisson’s Ratio at Room Temperature. ASTM International, 2010.
- [47] B. S. Yilbas, S. Akhtar, and S. Z. Shuja. *Laser Forming and Welding Processes*. Springer International Publishing, Switzerland, 2013.



- [48] T.-L. Teng and C.-C. Lin. Effect of welding conditions on residual stresses due to butt welds. *International Journal of Pressure Vessels and Piping* 75, (1998) 857–864.
- [49] A. R. Kohandehghan and S. Serajzadeh. Arc welding induced residual stress in butt-joints of thin plates under constraints. *Journal of Manufacturing Processes* 13, (2011) 96–103.
- [50] L. Tall. Residual stresses in welded plates: A theoretical study. Fritz Engineering Laboratory, Department of Civil Engineering, Lehigh University, 1961.
- [51] K. Sindo. *Welding Metallurgy*. 2nd edition. John Wiley & Sons, New Jersey, 2003.
- [52] J. Barreda, X. Azpiroz, and A. Irisarri. Influence of the filler metal on the mechanical properties of Ti–6Al–4V electron beam weldments. *Vacuum* 85, (2010) 10–15.
- [53] R. R. Boyer. An overview on the use of titanium in the aerospace industry. *Materials Science and Engineering: A* 213, (1996) 103–114.
- [54] S. Wang and X. Wu. Investigation on the microstructure and mechanical properties of Ti–6Al–4V alloy joints with electron beam welding. *Materials & Design* 36, (2012) 663–670.
- [55] N. Saresh, M. G. Pillai, and J. Mathew. Investigations into the effects of electron beam welding on thick Ti–6Al–4V titanium alloy. *Journal of Materials Processing Technology* 192, (2007) 83–88.
- [56] Q. Yunlian, D. Ju, H. Quan, and Z. Liying. Electron beam welding, laser beam welding and gas tungsten arc welding of titanium sheet. *Materials Science and Engineering: A* 280, (2000) 177–181.
- [57] A. M. Irisarri, J. L. Barreda, and X. Azpiroz. Influence of the filler metal on the properties of Ti-6Al-4V electron beam weldments. Part I: Welding procedures and microstructural characterization. *Vacuum* 84, (2009) 393–399.
- [58] M. J. Donachie. *Titanium: a technical guide*. ASM international, 2000.
- [59] W. Lu, Y. Shi, Y. Lei, and X. Li. Effect of electron beam welding on the microstructures and mechanical properties of thick TC4-DT alloy. *Materials & Design* 34, (2012) 509–515.
- [60] J. A. Nelder and R. Mead. A simplex method for function minimization. *The computer journal* 7, (1965) 308–313.
- [61] C. Huang, Y. Pan, and T. Chuang. Effects of post-weld heat treatments on the residual stress and mechanical properties of electron beam welded SAE 4130 steel plates. *Journal of materials engineering and performance* 6, (1997) 61–68.